



UNIVERSITAT POLITÈCNICA DE CATALUNYA  
BARCELONATECH

Escola d'Enginyeria de Barcelona Est

# 3D PRINTING USING METALLIC ALLOYS IN THE SEMISOLID STATE

A Master Thesis

Submitted to

PROCOMAME Research Group

Department of Materials Science and Engineering

Barcelona East School of Engineering

**Universitat Politècnica de Catalunya**

By

**Issam BOUMEHDI**

Thesis to obtain a Double International Engineer's Degree:

*\*Máster Universitario en Ciencia e Ingeniería Avanzada de Materiales  
(Master's Degree in Advanced Materials Science and Engineering)  
Universitat Politècnica de Catalunya, Spain*

*\*Diplôme d'Ingénieur en Génie des Matériaux  
(Master of engineering in Materials Science and Engineering)  
Ecole Européenne d'Ingénieurs en Génie des Matériaux, France*

Advisor: Prof. Jessica Calvo Muñoz

Barcelona, January 2022



## Thanks

*This work was made possible thanks to the help of several people to whom I would like to express my deep and sincere gratitude:*

- *Ms. Jessica Calvo Muñoz, my professor and advisor within the UPC for her confidence, support, relevant explanations, attention and kindness throughout this period of my research internship.*
- *Mr. Crisanto Jose Villalobos Gutierrez for his availability, help and support.*

*I would also like to thank all the members of the **PROCOMAME Research Group** with whom I worked during this internship, from whom I learned many new things and with whom I had a very good experience that will remain etched in my memory.*

*And the best for last...!*

*A BIG THANK YOU to my **Dear Dad** and my **Dear Mom** to whom I owe my whole life! Without them this work would never have been possible. I love you so much!*

*I also want to thank my little sisters **Basmita** and **Maryama**, my grandparents and all my family and loved ones.*

*Moltes gràcies, Muchas gracias, Thank you so much, Merci beaucoup, Vielen Dank!*

*شکرا جزیلا!*



## Abstract

This research project focuses on 3D Printing using metallic alloys in the semi-solid state, a revolutionary theme in the field of Metal Additive Manufacturing. In this work, the use of alloys, particularly Aluminium 357.0-F, processed in the semi-solid state was explored as a novel technology aiming at reducing printing costs. This is a continuation of studies done previously on the creation of a 3D printer to extrude some metallic alloys, based on their thixotropic properties, and on the design of a specific induction heating system for the machine. The first step was to manufacture the coil designed formerly and validate experimentally the electromagnetic induction heating system. To do so, a 3D modelling of the nozzle and the coil was conducted on CATIA software as well as the creation, using 3D polymer printing technology, of a part that allows giving the exact geometry to the coil. The reasoning followed is to, first, perform various thermal tests only on the extruder without being mounted to the body of the printer to be able to evaluate the thermal profile of the interior wall. This allowed to better estimate the thermal profile inside the nozzle during the extrusion experiments. Several coils of different geometries were tested, and various extrusion experiments were done. The analyses with the OM and SEM for each case showed that the extruded material contained a dendritic microstructure, which means that the material was melted. This is due to the problems of conduction, convection and the complexity of properly controlling the internal thermal profile during extrusion. It will therefore be necessary to improve the design of the extruder in the future to be able to better control the temperatures and consequently succeed the extrusion in the semi-solid state.

## Resumen

Este proyecto de investigación se centra en la impresión 3D utilizando aleaciones metálicas en estado semisólido, un tema revolucionario en la fabricación aditiva de metales. En este trabajo, se exploró el uso de aleaciones, particularmente aluminio 357.0-F, procesadas en estado semisólido como una nueva tecnología destinada a reducir los precios de impresión. Esto es una continuación de los estudios realizados anteriormente sobre la creación de una impresora 3D para extruir algunas aleaciones metálicas, basándose en sus propiedades tixotrópicas, y en el diseño de un sistema de calentamiento por inducción específico para la máquina. El primer paso fue fabricar la bobina diseñada anteriormente y validar experimentalmente el sistema de calentamiento por inducción electromagnética. Por esta finalidad, se realizó un modelo 3D de la boquilla y la bobina en el software CATIA, así como la creación, utilizando la tecnología de impresión 3D de polímeros, de una pieza que permite dar la geometría exacta a la bobina. El razonamiento seguido es, en primer lugar, realizar varias pruebas térmicas sólo en la boquilla sin ser montada en el cuerpo de la impresora para poder evaluar el perfil térmico de la pared interior. Esto permitió estimar mejor el perfil térmico dentro de la boquilla durante los experimentos de extrusión. Se probaron varias bobinas de diferentes geometrías y se realizaron varios experimentos de extrusión. Los análisis con el Microscopio Óptico (OM) y el Microscopio Electrónico de Barrido (SEM por sus siglas en inglés) para cada caso mostraron que el material extruido contenía una microestructura dendrítica, lo que significa que el material se fundió. Esto se debe a los problemas de conducción, convección y a la complejidad de controlar adecuadamente el perfil térmico interno durante la extrusión. Por lo tanto, será necesario mejorar el diseño de la extrusora en el futuro para poder controlar mejor las temperaturas y, en consecuencia, tener éxito en la extrusión en estado semisólido.

## Resum

Aquest projecte de recerca es centra en la impressió 3D utilitzant aliatges metàl·lics en estat semisòlid, un tema revolucionari en la fabricació additiva de metalls. En aquest treball, es va explorar l'ús d'aliatges, particularment alumini 357.0-F, processats en estat semisòlid com a nova tecnologia destinada a reduir els preus d'impressió. Això és una continuació dels estudis realitzats anteriorment sobre la creació d'una impressora 3D per extruir alguns aliatges metàl·lics, basant-se en les propietats tixotròpiques, i en el disseny d'un sistema d'escalfament per inducció específic per a la màquina. El primer pas va ser fabricar la bobina dissenyada anteriorment i validar experimentalment el sistema d'escalfament per inducció electromagnètica. Per aquesta finalitat, es va realitzar un model 3D del filtre i la bobina al programari CATIA, així com la creació, utilitzant la tecnologia d'impressió 3D de polímers, d'una peça que permet donar la geometria exacta a la bobina. El raonament seguit és, en primer lloc, realitzar diverses proves tèrmiques només al filtre sense ser muntada al cos de la impressora per poder avaluar el perfil tèrmic de la paret interior. Això va permetre estimar millor el perfil tèrmic dins del filtre durant els experiments d'extrusió. Es van provar diverses bobines de diferents geometries i es van fer diversos experiments d'extrusió. Les anàlisis amb Microscopia Òptica (OM) i Miscroscopia Electrònica de Rastreig (SEM per les eves sigles en anglès) per a cada cas van mostrar que el material extruït contenia una microestructura dendrítica, cosa que significa que el material es va fondre. Això és degut als problemes de conducció, convecció i a la complexitat de controlar adequadament el perfil tèrmic intern durant l'extrusió. Per tant, cal millorar el disseny de l'extrusora en el futur per poder controlar millor les temperatures i, en conseqüència, tenir èxit en l'extrusió en estat semisòlid.

## Résumé

Ce projet de recherche s'intéresse à l'impression 3D des alliages métalliques à l'état semi-solide, une thématique révolutionnaire dans le domaine de la fabrication additive des matériaux métalliques. Dans cette étude, l'utilisation d'alliages, notamment l'Aluminium 357.0-F traité à l'état semi-solide, a été explorée comme une nouvelle technologie visant à réduire les coûts d'impression. Il s'agit de la suite des travaux réalisés précédemment sur la création d'une imprimante 3D pour extruder certains alliages métalliques, en fonction de leurs propriétés thixotropiques, et sur la conception d'un système de chauffage à induction spécifique pour la machine. La première étape consistait à fabriquer la bobine conçue précédemment et à valider expérimentalement le système de chauffage par induction électromagnétique. Pour ce faire, une modélisation 3D de la buse et de la bobine a été réalisée sur le logiciel CATIA ainsi que la création d'une pièce qui permet de donner la géométrie exacte à la bobine à l'aide de la technologie de la fabrication additive des polymères. Le raisonnement suivi était d'effectuer, dans un premier temps, plusieurs tests thermiques uniquement sur l'extrudeuse sans être montée sur le corps de l'imprimante pour être en mesure d'évaluer le profil thermique de la paroi intérieure. Cela a permis de mieux estimer le profil thermique à l'intérieur de la buse lors des expériences d'extrusion. Plusieurs bobines de différentes géométries ont été testées et diverses expériences d'extrusion ont été réalisées. Les analyses effectuées au MO et au SEM pour chaque cas ont montré que le matériau extrudé contenait une microstructure dendritique, ce qui signifie que le matériau a fondu. Ceci est dû aux problèmes de conduction, de convection et à la complexité de contrôler correctement le profil thermique interne pendant l'extrusion. Il est donc nécessaire d'améliorer la conception de l'extrudeuse dans l'avenir pour pouvoir mieux contrôler les températures et donc réussir l'extrusion à l'état semi-solide.





## Table of Contents

Thanks .....	3
Abstract .....	5
Resumen .....	6
Resum .....	7
Résumé .....	8
List of figures .....	12
List of tables .....	14
Nomenclature.....	14
Introduction .....	15
1. Additive manufacturing.....	16
1.1. Definition .....	16
1.2. The generic AM process .....	17
1.3. Why AM? .....	20
1.3.1. Geometric complexity .....	20
1.3.2. A shorter manufacturing time .....	21
1.3.3. Material complexity .....	22
1.3.4. Other advantages and some negative points.....	23
1.4. Process categories .....	23
1.4.1. Material jetting.....	23
1.4.2. Material extrusion.....	24
1.4.3. Binder jetting.....	25
1.4.4. Powder bed fusion.....	25
1.4.5. Directed energy deposition.....	26
1.4.6. VAT photopolymerisation .....	27
1.4.7. Sheet lamination.....	28
1.5. Economic approach .....	29
2. Semi-solid state .....	30
2.1. Definition .....	30
2.2. Some advantages of the semi-solid forming .....	32
2.3. Link with the study.....	33
3. Induction heating.....	36
3.1. Definition & Physical phenomenon.....	36
3.2. Mathematical approach of the electromagnetic induction heating.....	37

3.2.1. Electromagnetic transfer between inductor and charge .....	37
3.2.2. Thermal effects .....	39
4. Experimental procedure .....	40
4.1. 3D printing machine .....	40
4.2. Heating trials .....	45
4.3. Extrusion trials .....	47
4.4. Samples preparation.....	47
4.4.1. The cut of the sample .....	47
4.4.2. Mounting.....	48
4.4.3. Polishing.....	48
4.5. Final heating and extrusion trials .....	50
5. Results and discussion.....	51
5.1. Coil conception.....	51
5.2. Heat experiments .....	54
5.2.1. Experiment 1 .....	54
5.2.2. Experiment 2 .....	55
5.3. Extrusion experiments .....	56
5.3.1. Experiment 1 .....	56
5.3.2 Samples analysis.....	57
5.3.3. Experiment 2 .....	67
5.4. New heating tests & the third extrusion experiment.....	68
Conclusion.....	71
References .....	72
Annex A .....	74
Annex B.....	75

## List of figures

Figure 1: Principle of additive manufacturing. [3] .....	16
Figure 2: 3D CAD model of a sample car rim. [6].....	17
Figure 3: Principle of STL format. [7].....	18
Figure 4: Conversion to STL. [5].....	18
Figure 5: Build step. [8].....	19
Figure 6: Generic process of AM. [4].....	20
Figure 7: The idea of 'Complexity for Free'. [11].....	21
Figure 8: Illustration of material complexity enabled by AM. [2].....	22
Figure 9: Illustration of the material jetting process (Polyjet technology). [2] .....	24
Figure 10: Illustration of the material extrusion process – Case of a two-nozzle. [2] .....	24
Figure 11: Illustration of the binder jetting process (Polyjet technology). [2] .....	25
Figure 12: Illustration of the powder bed fusion process. [2] .....	26
Figure 13: Illustration of the directed energy deposition process. [2].....	27
Figure 14: Illustration of the VAT photopolymerization process. [2] .....	27
Figure 15: Illustration of the sheet lamination process. [2] .....	28
Figure 16: Uses of AM processes. [2] .....	28
Figure 17: Metal AM market in 2019. [15] .....	29
Figure 18: Total AM market size. [16] .....	30
Figure 19: Binary diagram. [18].....	30
Figure 20: Schematic illustration of equiaxed dendritic growth. [21] .....	32
Figure 21: Schematic illustration of basaltic dendritic microstructure. [20].....	32
Figure 22: Dendritic growth during solidification. [9] [23] .....	34
Figure 23: Evolution of the microstructure during solidification with a shear stress. [9][22].....	34
Figure 24: Microstructure along the extruder body in rheocasting. [9] .....	35
Figure 25: Microstructure along the extruder body in thixotropic case. [9] .....	35
Figure 26: The principle of induction heating. [27].....	37
Figure 27: The 3D printing machine and its components.....	41
Figure 28: The extruder body, the nozzle, and the 8 bolts. ....	41
Figure 29: The hydraulic piston.....	42
Figure 30: The pump.....	42
Figure 31: The manual console.....	42
Figure 32: The pressure regulator and the manometer. ....	42
Figure 33: The building platform.....	43
Figure 34: The electronic board for the control of the process. ....	43
Figure 35: The heating system. ....	43
Figure 36: YUELON model HF15-A inductor. ....	44
Figure 37: The water-cooling system.....	44
Figure 38: PID Eurotherm serie 3204. ....	44
Figure 39: The positioning of the thermocouples inside the nozzle.....	45
Figure 40: TC-08 thermocouple data logger. ....	46
Figure 41: Setting up the experiment. ....	46
Figure 42: Aluminium samples. ....	47
Figure 43: the general scheme of the cutes made. ....	47
Figure 44: Struers LaboPress-3 hot coating machine. ....	48
Figure 45: "Struers LaboPol-5" polisher.....	48
Figure 46: Buehler Vibromet 2 vibratory polisher. ....	49

Figure 47: Ultrasonic cleaner.....	49
Figure 48: The SR-80 Universal Welder and its accessories.....	50
Figure 49: Four 4 thermocouples welded inside the nozzle.....	50
Figure 50: Thermal insulation wool installed above the nozzle. ....	51
Figure 51: The old extrusion head. [9].....	51
Figure 52: The new model of the nozzle.....	52
Figure 53: 3D model of the nozzle inside the coil.....	52
Figure 54: 3D model of the part printed. ....	53
Figure 55: The polymer 3D printer used (left) and the PLA part printed (right). ....	53
Figure 56: The nozzle inside the coil. ....	53
Figure 57: The thermocouple closest to the extruder outlet. ....	54
Figure 58: The thermal profile of the first heat experiment.....	54
Figure 59: The thermal profile of the second heat experiment. ....	55
Figure 60: Experiment 1 of extrusion. ....	57
Figure 61: The sample to analyse. ....	57
Figure 62: The three observation points A1, B1 and C1 in sample 1. ....	58
Figure 63: Point A1 observed with the au OM. ....	58
Figure 64: Point B1 observed with the au OM. ....	58
Figure 65: Point C1 observed with the au OM. ....	59
Figure 66: An example of images obtained with the SEM. ....	59
Figure 67: Spectrum of the area in Figure 66. ....	60
Figure 68: The four observation points A2, B2, C2 and D2 in sample 2.....	60
Figure 69: Point A2 observed with the au OM. ....	61
Figure 70: Point B2 observed with the au OM. ....	61
Figure 71: Point C2 observed with the au OM. ....	61
Figure 72: Point D2 observed with the au OM.....	62
Figure 73: Silicon precipitation in point C2 observed with the au OM (x50). ....	62
Figure 74: An example of images obtained with the SEM. ....	63
Figure 75: Spectrum of the area in Figure 74. ....	63
Figure 76: SI zone observed with SEM. ....	64
Figure 77: Spectrum of the area in Figure 76. ....	64
Figure 78: Average grain size calculations for sample 2. ....	65
Figure 79: Calculations for point 1. ....	65
Figure 80: Calculations for point 2. ....	65
Figure 81: Calculations for point 3. ....	66
Figure 82: An example of images obtained with the OM for sample 4.....	66
Figure 83: An example of images obtained with the OM for sample 3.....	67
Figure 84: New coil of 3 spirals.....	68
Figure 85: Dendritic microstructure in the second extrusion experiment. ....	68
Figure 86: The thermal profile of the first new heat experiment. ....	69
Figure 87: The thermal profile of the second new heat experiment.....	70
Figure 88: The result of the last extrusion experiment. ....	70

## List of tables

<i>Table 1: Other advantages and some negative points of AM. [12]</i> .....	23
<i>Table 2: Examples of applications of induction heating. [26]</i> .....	37
<i>Table 3: Chemical composition of the area in Figure 66.</i> .....	60
<i>Table 4: Chemical composition of the area in Figure 74.</i> .....	63
<i>Table 5: Chemical composition of the area in Figure 76.</i> .....	64

## Nomenclature

**AM:** Additive manufacturing.  
**SEM:** Scanning electron microscopy.  
**CAD:** Computer aided design.  
**FDM:** Fused Deposition Modelling.  
**EBM:** Electron Beam Melting.  
**Al357.0-F:** Aluminium 357.0-F.  
**PLA:** Polylactic acid.  
**PID:** Proportional Integral Derivative  
**OM:** Optical microscopy  
**HF:** Hydrofluoric acid.

## Introduction

Nowadays, Additive Manufacturing or 3D Printing, which consists of the creation layer by layer of an object based on a specific numerical designed model, has become a very famous technological trend in the field of materials science and engineering. In past years, many technologies were developed for AM of metallic materials. However, the majority of them are expensive and require a high-energy source, such as laser or electron beam, to achieve good sintering of a metallic powder.

In this sense, this research project focuses on a new and original Metal AM process that aims to extrude metallic alloys in the semisolid state, principally the Aluminium 357.0-F, using a special 3D printer machine designed for that. In other words, the main objective is to achieve the additive manufacturing of metallic alloys in the semisolid state.

The development consists basically of the validation, experimentally, of the inductor heating system designed in previous projects, and then the realisation of the extrusion experiences. The broad lines initially expected of this work are:

- Fabricating and implementing the heating system previously designed numerically.
- Validating experimentally the heating induction system and working on its amelioration.
- Realising extrusion experiences.
- Characterising the microstructure of the extruded samples to verify if the material melted or not during the 3D printing using Light Microscopy (LM) and Scanning Electron Microscopy (SEM) technologies.
- Giving suggestions to improve this AM process and try to avoid the melting problems of the aluminium alloy during printing and thus, achieve the main objective of this major research project which is to extrude the material in its semi-solid state.

# 1. Additive manufacturing

## 1.1. Definition

Standard NF E 67-001 [1] defines additive manufacturing as “the set of manufacturing processes that enable joining materials to create physical objects from 3D model data, layer by layer, as opposed to subtractive manufacturing methodologies”. [2]

However, while the term “additive manufacturing” (AM) is widely used in science today, it is not uncommon for other terms to be used to refer to the same technology. The most recurrent, although sometimes considered as over-simplifications, are:

- 3D printing.
- Additive layer manufacturing.
- Digital manufacturing.
- Rapid manufacturing.
- Rapid prototyping.

The physical principle on which the AM is based has been in use as early as the late 19th century in the fields of photo sculpture and topography. It consists in making a product through a successive stacking of strata. The preparation of the digital model allows defining the sections of the 3D object to be made by its successive decoupling by parallel planes.

The distance between each section is the thickness of a layer. To reconstruct the object, the sections are stacked sequentially on top of each other (Figure 1). [2]

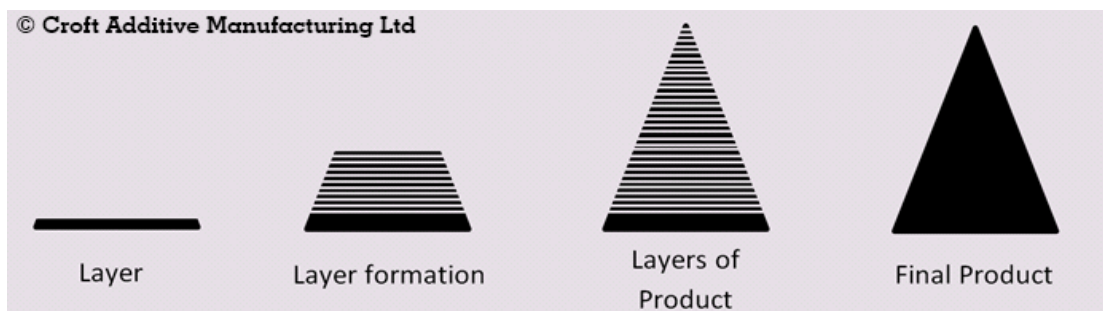


Figure 1: Principle of additive manufacturing. [3]

3D printing is, therefore, the result of a generative manufacturing process consisting of two repeated steps until the final product is produced:

1. Generate a layer of material following a defined thickness and set outline. The material is deposited only where it is needed.
2. Make the new layer by adding material above the previous one. This can be summarised as step production (Figure 1). [2]



Thus, because of this principle of material's addition, the AM revolutionizes the so-called traditional manufacturing techniques that are:

- Processes by removing material or subtractive manufacturing (such as machining, milling, and boring) where the product is made from a blank, from which the material will be gradually removed in order to give it a final shape.
- Forming processes (such as casting, rolling, bending and forging) in which the material is brought to a liquid state and poured into a mould or subjected to plastic deformation. [2]

## 1.2. The generic AM process

The additive manufacturing process could be explained in 8 different steps. Five of them involve a succession of information conversions through different software. These steps start with the virtual CAD and finish with the physical resultant object. The type and the different properties of the desired product will involve AM in various ways and not to the same degrees. In other words, small and relatively simple products may only require the 3D printing to visualise models, while more complex and larger objects may involve AM during different steps and iterations throughout the development process because of their greater engineering content. In addition, early stages of the product fabrication process may only demand rough objects, with AM being used thanks to the rapidity at which they can be created. Later in the process, parts may require some special cleaning and post-processing works such as sanding, painting and surface preparation before they are used. Here, the AM is very useful because of the complexity of form that can be printed without the necessity to consider tooling. [4] [5]

### Step 1 : CAD

The first step in the additive manufacturing process is the creation of a CAD (computer-aided design) model using computer software such as CATIA and SOLIDWORKS to create, modify and analyse three dimensional drawings of physical objects [5]. As an example, the CAD design for a car rim can be observed in Figure 2.

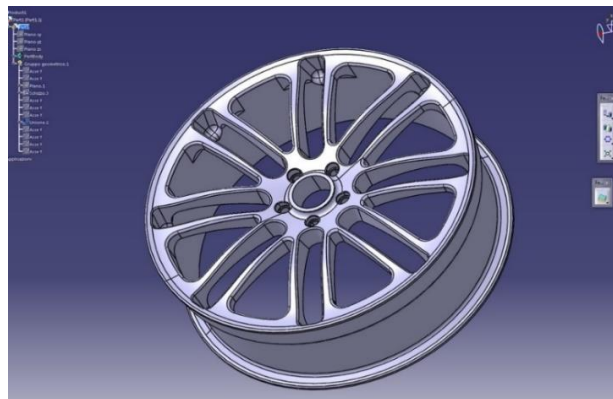


Figure 2: 3D CAD model of a sample car rim. [6]

## Step 2 : Conversion to STL

Once the model is created, it is transformed into .STL format (or .AMF and .3MF, newer formats), which is a triangulated representation in a 3D CAD model. [5]

For example, for a simple model, such as the box shown in the left of Figure 3, its surfaces may correspond approximately to twelve triangles. More complex is the surface, more triangles are produced (The right of Figure 3). [7]

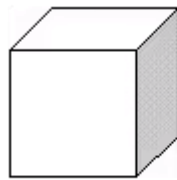


Figure 1

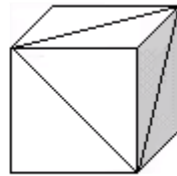


Figure 2



Figure 3

Figure 3: Principle of STL format. [7]

This file describes the external closed surfaces of the original CAD model, and it also forms the basis of the slices calculation. [4] Figure 4 schematizes the principle of the conversion to STL file.



Figure 4: Conversion to STL. [5]

## Step 3 : Transfer to AM Machine

In this step, the STL file describing the part is transferred to the 3D printer. Here, there may be some general manipulation of the file in order to obtain correct position, size, and orientation for building. [4]

## Step 4 : Machine setup

At this stage, each technology will require different processes of preparation, calibration and configuration. These settings serve to build different parameters such as the energy source, material constraints, timings, layer thickness, etc. One of the very important steps in the preparation of the machine will be the cleaning of residues from the previous production. [5] [4]

## Step 5 : Build

In the part production phase, the machine will automatically execute the commands to build, layer by layer, the slice defined in previous steps. The printer can largely carry on without special supervision. However, at this time, a superficial monitoring needs to take place to ensure no errors have taken place like power or software glitches, running out of material, etc. [5] [4] Figure 5 shows an example of part being manufactured by 3D printing.

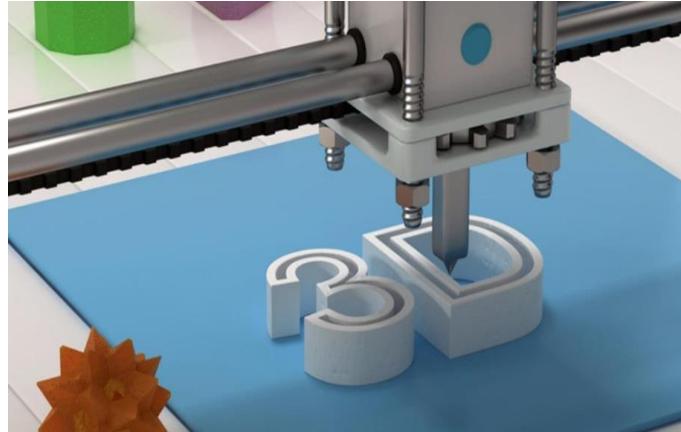


Figure 5: Build step. [8]

## Step 6 : Removal

Once the printing has been completed, the part must be removed from the print bed. Sometimes, this operation may require interaction with the 3D printing machine, which can have safety interlocks to guarantee for example that there are no actively moving parts or that the operating temperatures are sufficiently low. [4]

In the case of using powder, additional steps and extreme caution should take place to avoid material loss and health problems because of the inspiration of particles. [9]

## Step 7 : Post-processing

The post-treatment will be different for each technology, but most of the time, cleaning and treatment will be required to improve the surface. In some cases, no post-process will be needed. [5]

Among the operations that can be used during post-treatment:

- Impregnation of porous parts.
- The removal of supports, if applicable.
- Thermal stress relief to allow a relaxation of any residual stress in metal parts.
- Densification treatments, such as Hot Isostatic Pressing (HIP), applied to increase the density of parts.

- Surface treatments and superfinishing, carried out manually or automatically, linked to the existence of the stair-stepping effect inherent in the production by layer-by-layer. [2]

## Step 8 : Application

Parts are now ready to be used. [4]

All this 8 AM stages can be summarised and illustrated in the following Figure 6:

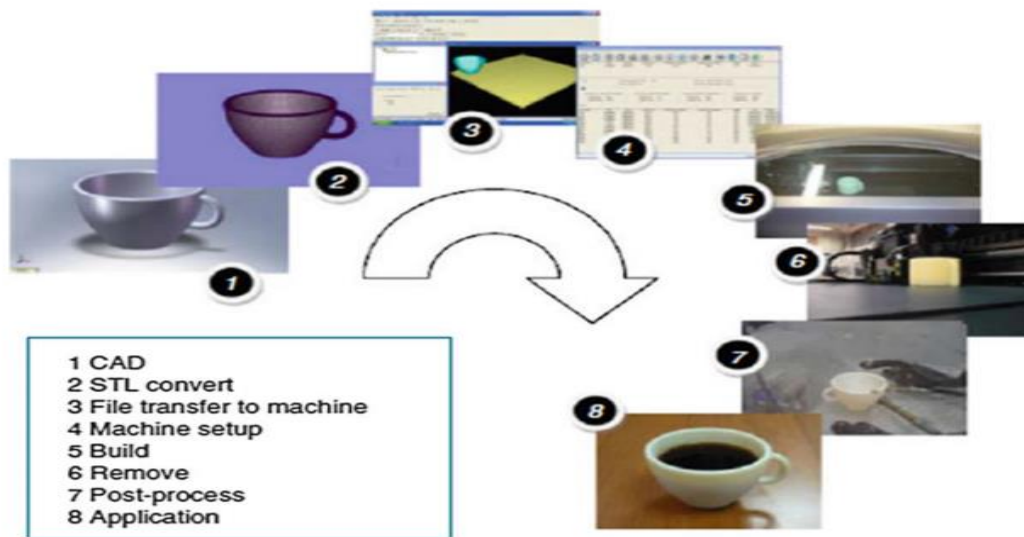


Figure 6: Generic process of AM. [4]

## 1.3. Why AM?

Thanks to the AM, the blanks inherent and dedicated tooling in traditional processes has become unnecessary, and the constraints related to their design and production are then lifted which permit saving time and money. Thus, AM offers unique possibilities and permits the achievement of complex shapes such as inclusions and cavities which could not be made by processes like machining. [2]

### 1.3.1. Geometric complexity

Not to focus solely on how AM can reorganise existing parts or reproduce the results of traditional processes is a key and a very important strategy during the assessment of innovative opportunities in additive manufacturing. The main question here is how additive techniques can be used to achieve results that are impossible or unaffordable by subtractive processes. Design freedom offers many opportunities. Designers and engineers can take advantage of almost endless options to improve tools designs.

When composed of multiple parts, the ability to consolidate the design minimises the negative assembly impacts and material costs. In addition, the possibility to incorporate complex features allows faster production of highly functional parts, while limiting defects and allowing free shapes design. For example, in the case of a cooling system design, ergonomics can be included in the design to improve the comfort of the technicians, the processing cycle time as well as the ease of accessing and storing tools. [10]

On the other hand, as it is shown in Figure 7, for small series production, increasing geometric complexity causes exponentially increasing costs in conventional production technologies cases. Nevertheless, manufacturing costs for 3D printing technologies like SLM do not normally increase with higher complexity, except in a few cases where higher geometric complexity requires higher pre-processing costs of SLM, for example: scanning strategy, backing and platform assembly. At the same time, high complexity often involves lower build volumes, which reduces the process time for SLM and permits the equality of the additional pre-processing costs. [11]

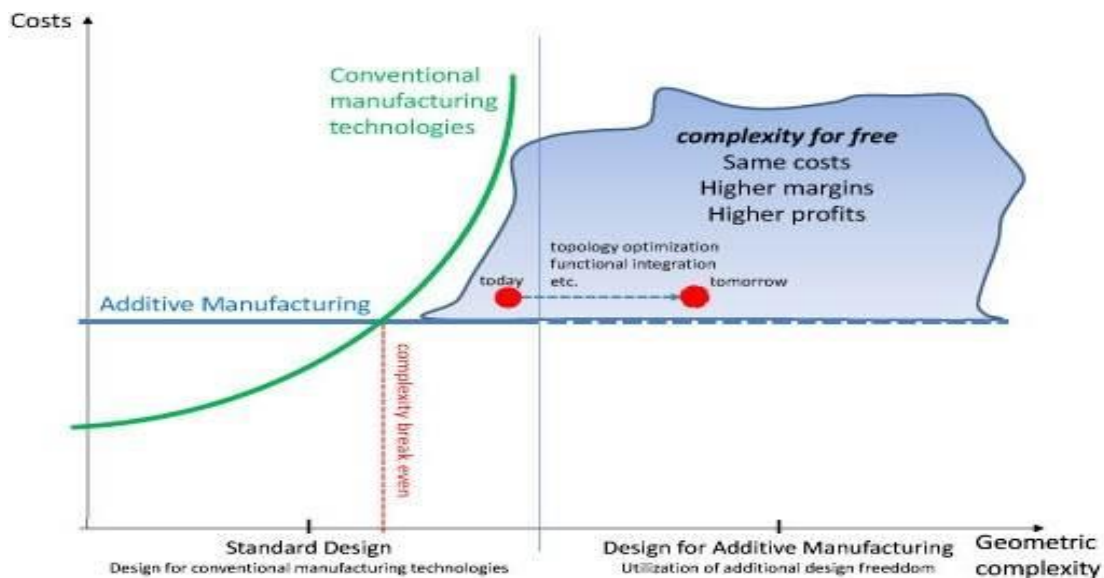


Figure 7: The idea of 'Complexity for Free'. [11]

### 1.3.2. A shorter manufacturing time

Additive manufacturing reduces the complete product development cycle, it is a real engine for innovation. Companies sometimes choose to delay or cancel product design updates because of the need to invest in new tools. By reducing the production time of the tooling and allowing rapid updates, additive manufacturing allows companies to replace and improve their tooling more frequently and easily. Having an in-house additive manufacturing system also shortens the supply chain and reduces, or even cancels sometimes, the risk of receiving defective tools. [10]

### 1.3.3. Material complexity

A multi-material part is a part that is formed with at least two materials whose distribution changes with width. Figure 8 illustrates two principles, continuous and discontinuous distribution, applied to a sports shoe sole prototype: [2]

- In the first case, the composites materials obtained are called Functionally Graded Materials (FGM), whose microstructure and composition change gradually across the part, with a variation in mechanical properties. The overall performance of the components taken separately is then lower than that of the material. [2]
- Discontinuous distribution enables parts to be obtained with stacked single-material areas. The material complexity obtained here is more elementary due to the lower performance obtained than that of the FGM. [2]

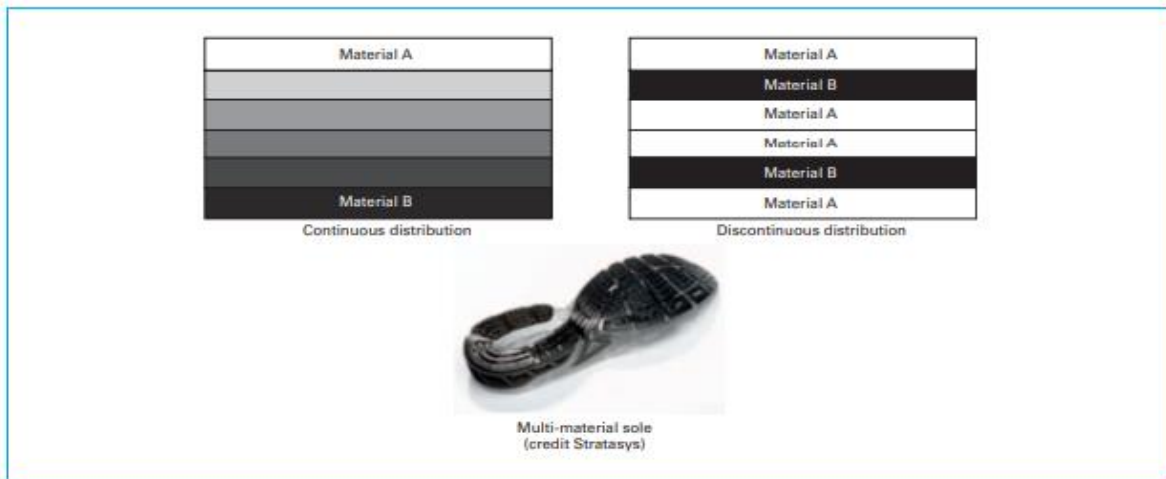


Figure 8: Illustration of material complexity enabled by AM. [2]

The potential of AM in the realisation of these multi-material parts has become self-evident. It is possible to achieve any composition at all, providing the part with unique chemical, mechanical or thermal properties, because within a single layer, the material is deposited simultaneously or point by point. [2]



### 1.3.4. Other advantages and some negative points

Advantages	Disadvantages
<ul style="list-style-type: none"><li>• Forms freedom;</li><li>• Lightening of parts;</li><li>• Customization;</li><li>• Disposal of assemblies;</li><li>• Materials economy;</li><li>• Production of a wide variety of parts with a single printer;</li><li>• Repair parts.</li></ul>	<ul style="list-style-type: none"><li>• Bad surface state of the final object (for example, the presence of roughness and staircase effect);</li><li>• Post-treatment takes longer than in the case of machining;</li><li>• Unreliability.</li></ul>

Table 1: Other advantages and some negative points of AM. [12]

## 1.4. Process categories

Various 3D printing processes have been developed and introduced in trade by industrial companies, such as Z Corporation, 3D Systems, Optomec and Stratasys in the USA, Electro Optical Systems (EOS) in Germany, Arcam in Sweden, and MCP Tooling Technologies in the UK. A classification system was established as part of the NF ISO 17296-2 [13] standard. It is based on the classification, in the same category, of processes which use a similar machine architecture and for which the physical transformation processes of the materials are identical. [2] [12]

So, the AM processes is classified into seven categories:

### 1.4.1. Material jetting

The material jetting process works on the same principle as inkjet printers. It consists in depositing drops of material from a nozzle that moves horizontally on the surface of the manufacturing area. The solidification is produced using ultraviolet light (UV).

Two types of materials can be used: [12] [2]

- Waxes deposited in liquid form which will constitute the part when cooled.
- Photosensitive resins which, once deposited, are polymerised by the UV light.

The most relevant advantage of the material jetting technology is the possibility to produce multi-material parts and introduce colour. Indeed, about 60 types of materials may be used which means that it is possible to obtain various prototypes in order to simulate the behaviour of objects created from standard or technical polymers by injection in functional tests. [2]

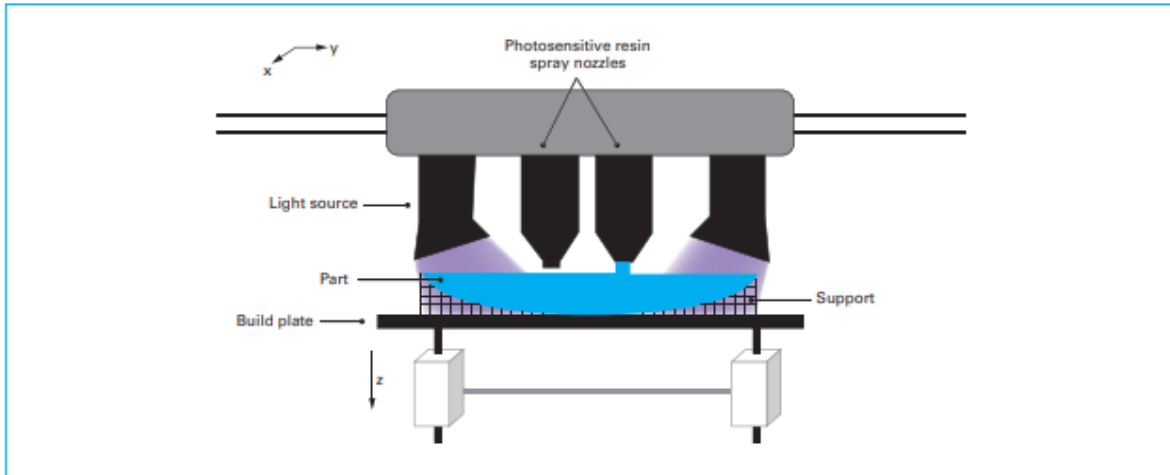


Figure 9: Illustration of the material jetting process (Polyjet technology). [2]

### 1.4.2. Material extrusion

This process involves depositing the material, previously heated above its melting point, layer by layer through a nozzle (or spinneret) onto the surface of the manufacturing area, which then cools and solidifies. Solidification of the material on the previous layer is almost immediate. The nozzle can move in the three spatial directions. Material extrusion was first applied to thermoplastic polymer materials (Fused Deposition Modelling, FDM process).

FDM is the main used 3D printing process in the world due to its low purchase price, especially for polymer FDM, which makes it accessible to all companies and the general public. [12] [2]

In the case of two-nozzle machines, as in Figure 10 below, one can be used to deposit the principal material and the other is used as a support material. The latter is cheaper and easier to detach from the part without causing damage to its surface, and it can be also used to create parts with two different materials without support. [2]

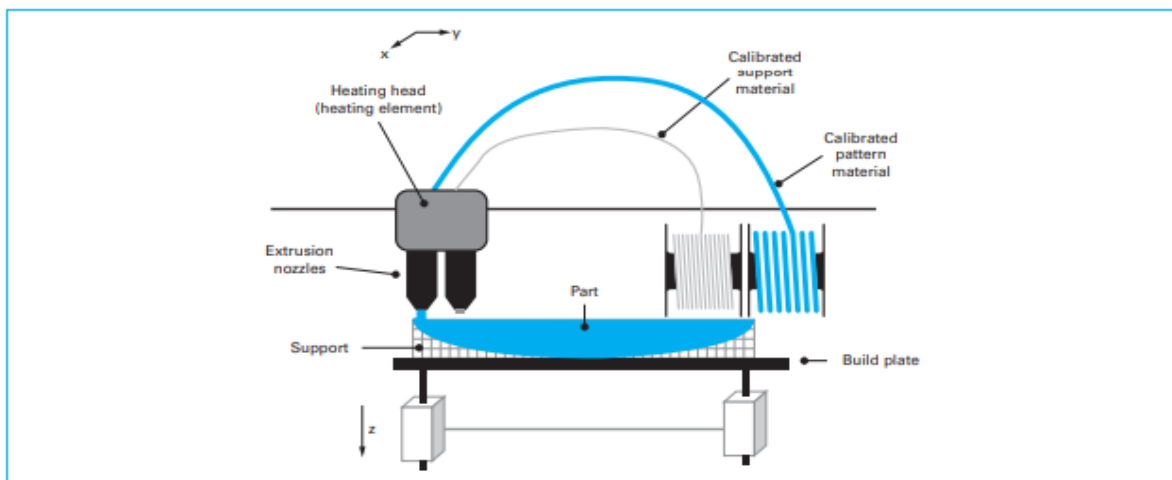


Figure 10: Illustration of the material extrusion process – Case of a two-nozzle. [2]



### 1.4.3. Binder jetting

Binder jetting is a process very close to the material jetting one. Appeared in 1993 at the Massachusetts Institute of Technology with the name of 3D Printing (3DP). It is based on the use of print heads, exactly like material jetting, here to project a liquid binder onto a powder bed building thus the construction material as Figure 11 shows. The unbound powder serves as a support for the part. Different types of materials can be used here : polymers, metals and ceramics. Indeed, it is possible to produce coloured parts because of the possibility to combine drops of coloured binder. However, the main disadvantage of Binder jetting is that the products obtained are fragile, which generally require post-treatment like sintering or infiltration and use in applications without high mechanical strain. [2]

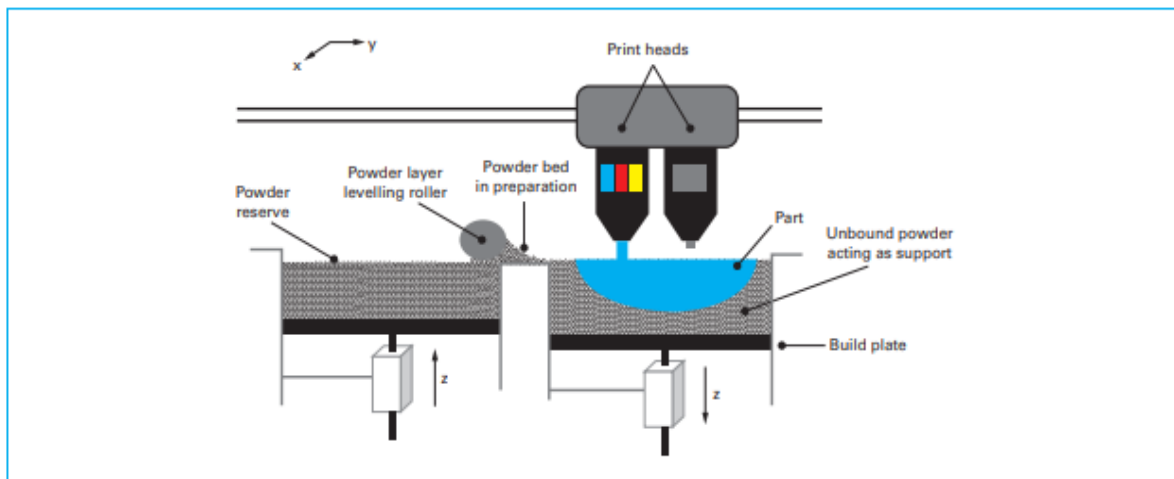


Figure 11: Illustration of the binder jetting process (Polyjet technology). [2]

### 1.4.4. Powder bed fusion

Generally speaking, Powder bed fusion requires either an electron beam (restricted to conductive materials) or a laser roller to melt the raw material (powder in this case) layer by layer.

The principle of this AM process, as illustrated in Figure 12, consists in the utilisation of thermal energy to melt a thin layer of powder, previously spread by a roller on a build plate. In Powder bed fusion, it is very important to suitably control the protective atmosphere within the build chamber. [2] [12]

In this process, there are three main categories: [2]

- EBM or Electron Beam Melting of metal powder which is a technique limited to conductive materials. The surface of final products here is bad due to the electron beam being wider than a laser beam and it is mandatory to preheat the powder bed in order to limit thermal gradients and therefore residual stresses.

- Laser sintering of thermoplastics polymer powders uses CO<sub>2</sub> lasers (power of a few tens of Watt). In February 2014, the public domain received the first patents protecting this technology.
- Laser metal powder melting uses YAG lasers (100 W to 1 kW). The layer thicknesses are in the order of a few tens of microns (20 to 100 μm according to the manufacturers).

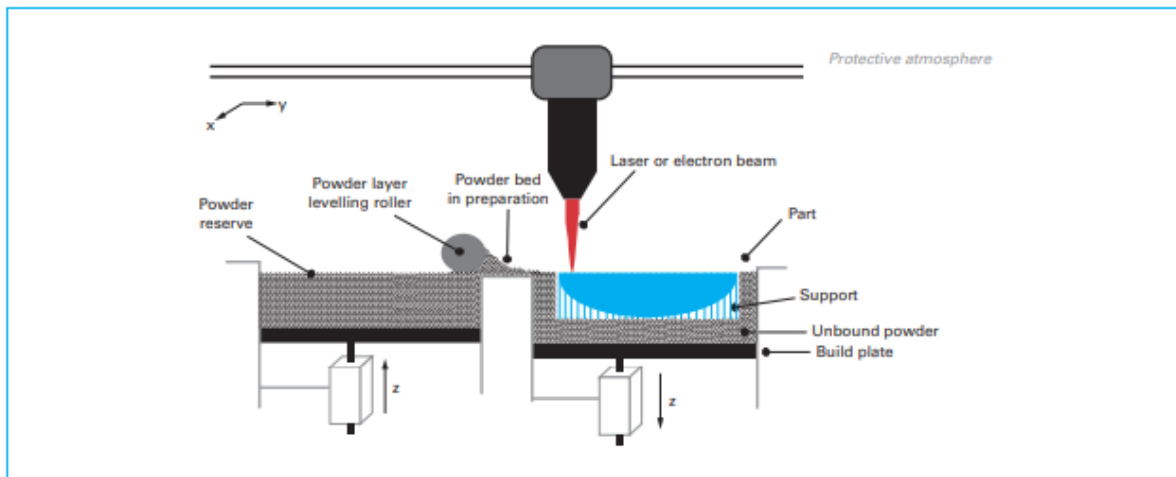


Figure 12: Illustration of the powder bed fusion process. [2]

#### 1.4.5. Directed energy deposition

Direct energy deposition is an AM process derived from laser coating techniques. It consists of the melting of a surface with a source of energy accompanied by a simultaneous contribution of a material filament or a powder jet in the molten zone, with the necessity of the presence of protective gas. The accuracy of the products obtained is lower than that obtained with powder bed fusion processes, and the thickness of the layer is more or less 500 μm. [2]

It is possible to use this process for ceramics and polymers, but is principally used with metals, in either wire or powder. [14]

Figure 13 below illustrates this process:

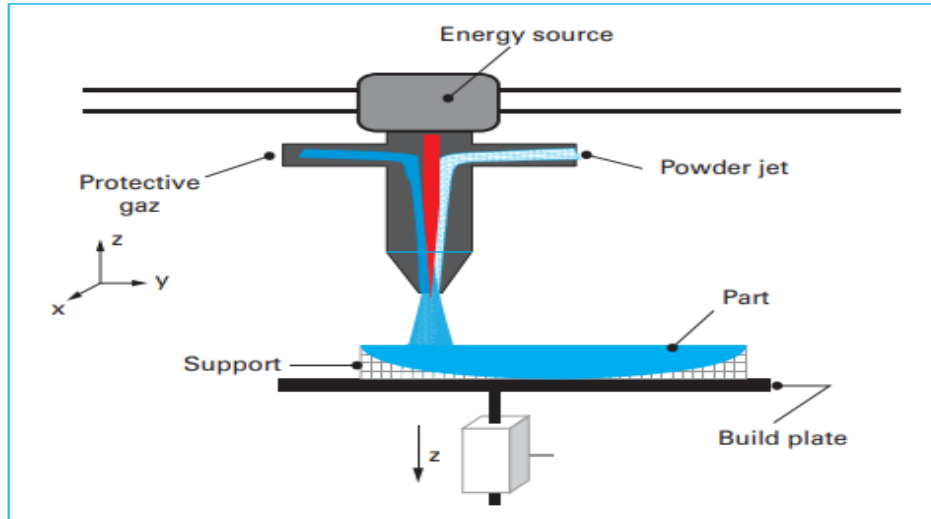


Figure 13: Illustration of the directed energy deposition process. [2]

#### 1.4.6. VAT photopolymerisation

For the VAT photopolymerisation process (Figure 14), the action of a light source hardens, by polymerisation, a liquid photosensitive resin contained in a vat. Once a resin layer is polymerised, the build plate is moved vertically in z-direction by a determined distance previously set production parameters to repeat the cycle. The nature of the light source (UV light or Laser) and the movement direction of the plate are the origin of the variants of this process. [2]

Even if this process permits the obtention of a good precision (a few tens of microns) and a good superficial quality, the major negative point of it is about the raw material used, that is to say, the varieties of resin are limited, and its properties are lower than those of technical polymers. Indeed, ageing may make parts brittle over time. [2]

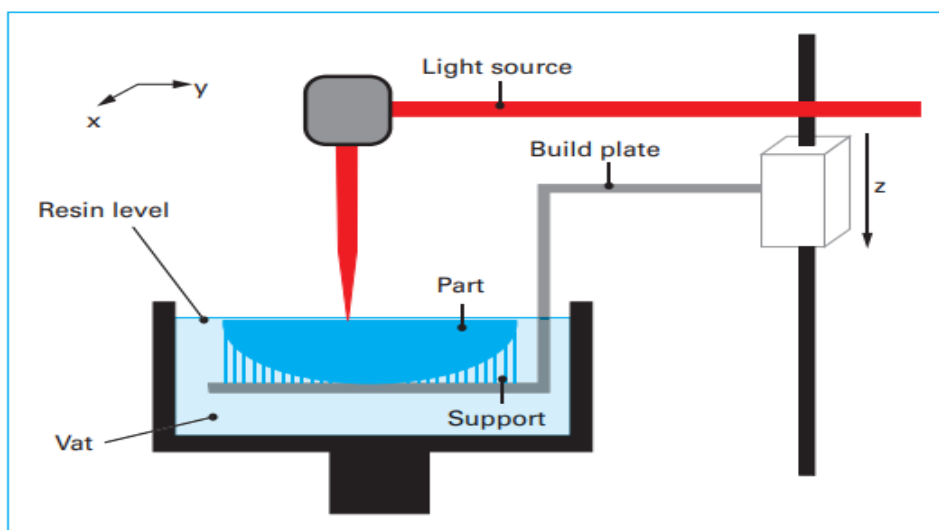


Figure 14: Illustration of the VAT photopolymerization process. [2]

### 1.4.7. Sheet lamination

Sheet lamination (Figure 15) is a process in which there exists a combination between the subtraction and addition of material. Plates or sheets of raw material are cut up with one of the different cutting systems such as a cutting tool, laser, or ultrasound, stacked and then linked together in order to form the part. All existing materials in the form of plates or sheets can be used. [2]

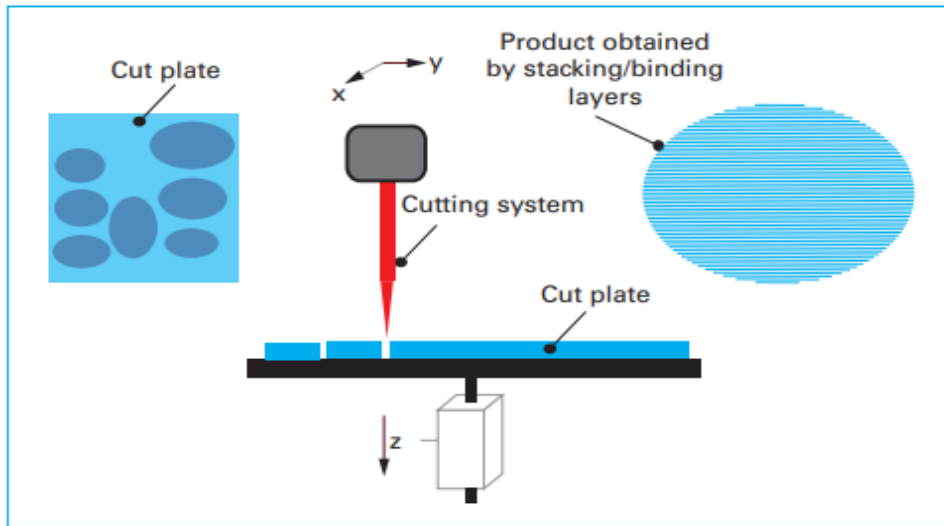


Figure 15: Illustration of the sheet lamination process. [2]

To sum up, Figure 16 below summarises the seven AM processes defined by NF ISO 17296-2.

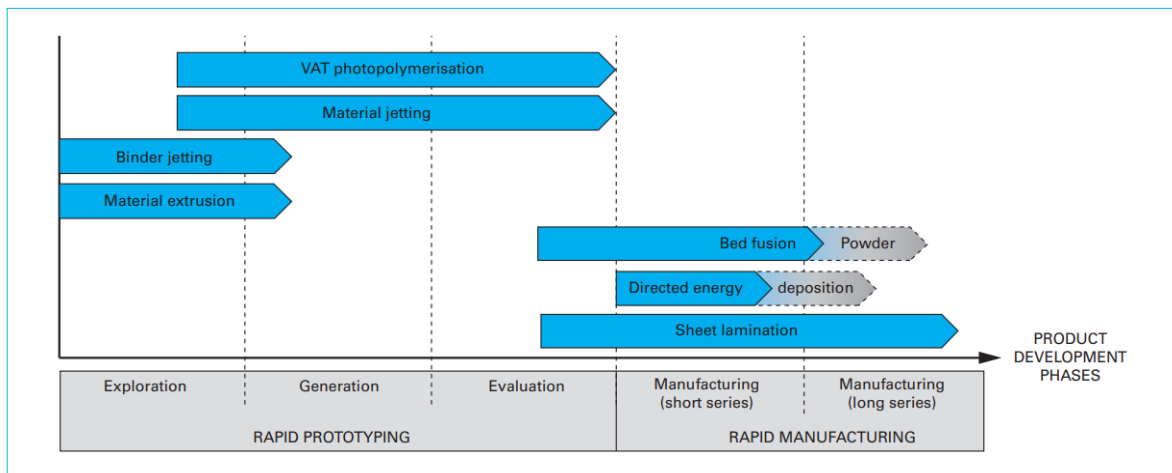


Figure 16: Uses of AM processes. [2]

Among the seven AM processes detailed above, only four are capable of directly manufacturing aluminium parts:

- Powder bed fusion.
- Binder jetting.
- Directed energy deposition.
- Sheet lamination.

Other categories may be useful for prototyping and manufacturing of models and tools.[12]

So, the main challenge of this “3D Printing using metallic alloys in the semisolid state, application to Aluminium 357.0-F” project is to achieve the extrusion of this aluminium alloy employing an induction heating system to reach the semi-solid range of the alloy.

### 1.5. Economic approach

In 2019, the metal AM market was dominated by powder bed fusion (54 %), and binder jetting technology is the second most dominating (16 %) (Figure 17). [9] [15]

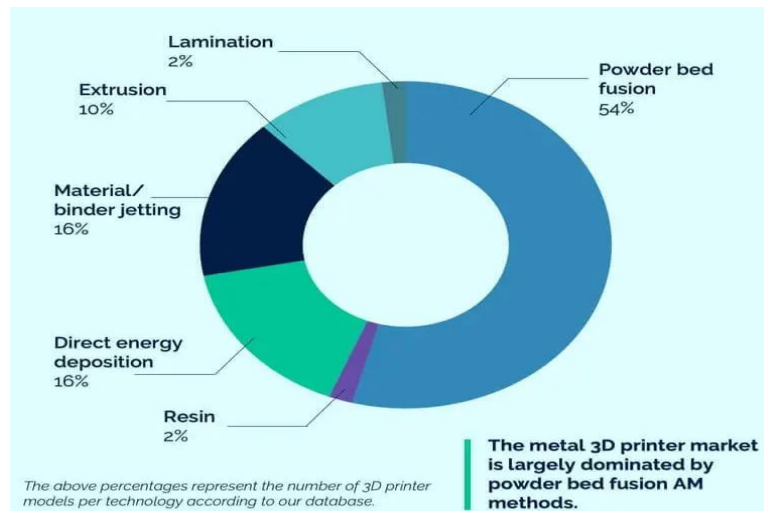


Figure 17: Metal AM market in 2019. [15]

This technology, which was born more than three decades ago, is now experiencing a meteoric rise. The 2018 year-end report of the American firm SmarTech Publishing indicates that no less than \$9.3 billion in revenues for the 2018 additive manufacturing market. By comparison, they were only 4.1 billion in 2014. This number, which covers hardware, software, materials and services, represents an 18% increase per contribution to 2017. In 2019, the 3D printing market reached \$11.2 billion and, therefore, exceeded the symbolic threshold of \$10 billion.

According to the same report, it was expected that in 2021, the AM market would reach \$16,9 (Figure 18). [16]

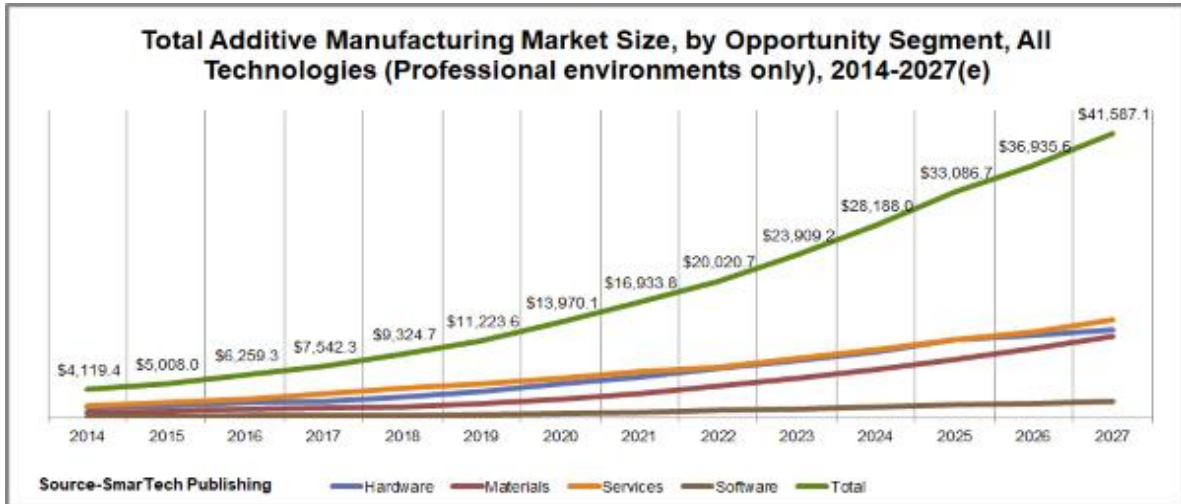


Figure 18: Total AM market size. [16]

## 2. Semi-solid state

### 2.1. Definition

In some shaping processes, particularly during the solidification and liquid sintering of powders that have different melting points, solid and liquid phases are present simultaneously. These two phases coexist when a previously solidified alloy is remelted. For solidification and remelting, in phase diagram, the domain of the coexistence of liquid and solid phases ( $L+\alpha$  and  $L+\beta$  domains) is limited by the liquidus and solidus lines, which also in equilibrium conditions, fixes their proportions and chemical compositions (Figure 19). [17]

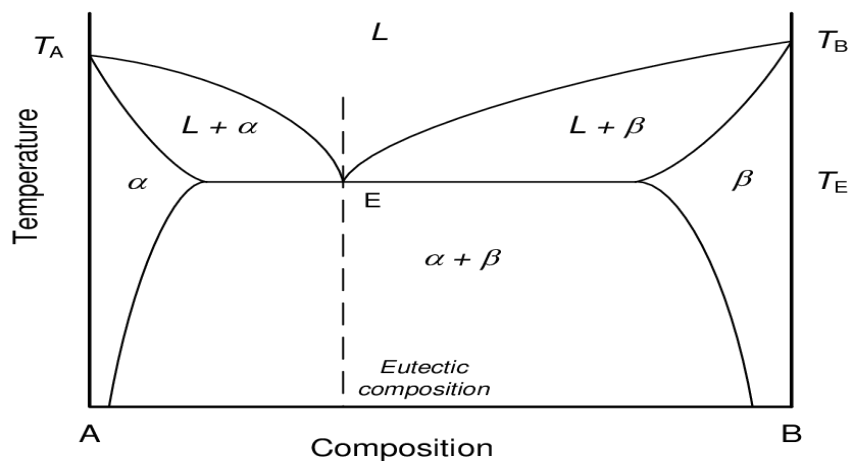


Figure 19: Binary diagram. [18]

Two cases are therefore distinguished: [9]

- “Slurry” composition: the liquid phase here presents the major proportion, and solid particles are in suspension within the liquid matrix.

- “Mush” composition: the solid phase here is in majority so the metal stays in shape.

It is relatively easy to determine which of them is present thanks to the rule on inverse segments by calculating, for a defined composition and temperature, the proportion of the solid and liquid phases. [9]

When solidifying a binary alloy with an initial solute concentration (minority alloying element)  $C_0$ , the solute concentrations at a defined temperature  $T$  of the liquid and solid phases ( $C_L$  and  $C_S$  respectively) are determined by knowing the phase diagram. The mass fractions of the two phases can then be deduced by applying the solute conservation principle. [17]

Two extreme hypotheses are generally used: [17]

- The total equilibrium of the solute in the liquid and in the solid, giving then a mass fraction of the liquid equal to:

$$f_L = \frac{C_0 - k C_L}{(1 - k) C_L} \quad (\text{Eq.1})$$

With  $k = C_S/C_L$  : the ratio of concentrations in a defined temperature  $T$ .

- Perfect homogenization in the liquid and no diffusion in the solid. The mass fraction of liquid  $F_L$  here is defined by the Scheil's equation, when  $k$  is constant:

$$f_L = \left( \frac{C_L}{C_0} \right)^{1/(k-1)} \quad (\text{Eq.2})$$

In usual conditions, the solidification structure of an ingot takes the form of equiaxed dendritic (Figure 20) or basaltic dendritic (Figure 21) depending on the cooling conditions. The basaltic structure is observed particularly when a gradient of temperature has an insufficient amplitude to lead solidification in the foreground: dendrites grow in the direction of heat flow. [17] [19] [20]

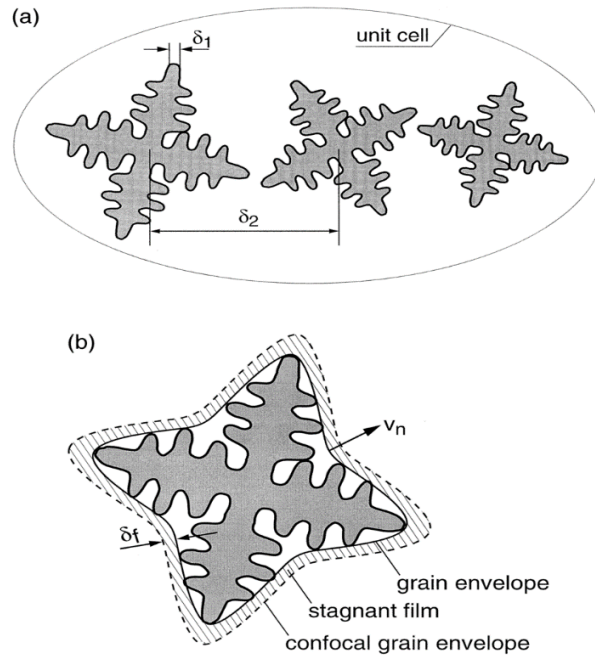


Figure 20: Schematic illustration of equiaxed dendritic growth. [21]

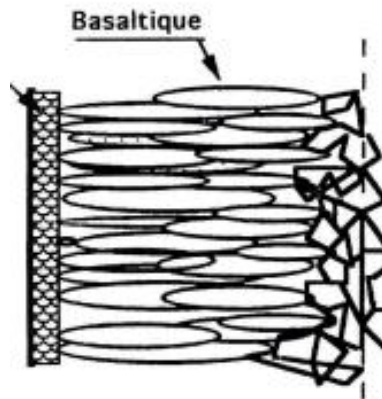


Figure 21: Schematic illustration of basaltic dendritic microstructure. [20]

## 2.2. Some advantages of the semi-solid forming

Semi-solid forming has many advantages which are mainly related to the structure of the material and its properties: [17]

- The lack of a continuous dendritic network, thanks to a structure essentially formed of approximately spherical primary globules, allows a homogeneous deformation of the jelly under low stresses without segregation of the liquid phase and formation of cracks either. [17]
- The control of the shape, mass and solid phase density fraction of the alloy load obtained directly by controlled solidification or by some specific treatment that requires partial remelting is easy. [17]



- The controllable viscosity that depends on the temperature, thus the solid phase density fraction, and forming conditions, can be adapted to the shaping technique to optimise the parameters like the conditions of slush flow in shells and force on tools. That makes it possible to produce thin parts close to the sides requiring only reduced machining. [17]
- During mixing, it is possible to add foreign particles like Al<sub>2</sub>O<sub>3</sub>, SiC, B<sub>4</sub>C and TiC to the semi-solid mixture which due to the relatively high viscosity of the jelly, will be evenly distributed. This leads to the production of composite materials that can be shaped under the same conditions. The semi-solid state also prevents some harmful chemical reactions between the alloy and the reinforcement, such as the formation of aluminium carbide in the case, for example, of SiC reinforcements. [17]
- The temperature of the material, which is lower than in the case of the liquid form, allows to minimise the contraction caused by the change of liquid-solid phase and thus to improve the metal state after solidification and also reduce the thermal energy produced during solidification. This last factor permits a reduction of the thermal shocks on the tools during shaping and, therefore, an increase of their service life. [17]

All these advantages could be put to use in different shaping processes at the scale of the laboratory or/and at industries, for example: gravity moulding, injection moulding, and extrusion that is the heart and the centre of the various studies carried out in this research project. [17]

### 2.3. Link with the study

It was chosen to work in the semi-solid state of metallic alloys because it is very adapted to the case of this project (thanks to the thixotropic properties of certain alloys), where it is necessary that the material to be 3D printed has certain specific properties, particularly for the viscosity, so that a layer can be printed without any spread of the material. It is therefore very important to pay attention to the microstructure of the solid phase because it will have a primary impact on the properties of the semi-solid state. [9] [22]

As mentioned before, a dendritic structure will be formed if the thermal gradient is positive in the liquid phase. In the solidification from the melt metal case, the steps of the dendritic growth are (Figure 22): [9]

1. The nucleation of a spheroidal solid within the liquid (a).
2. The appearance of a protrusion in order to maximise the surface (b).
3. The protrusion will grow and then create a primary dendrite (c).
4. On the first protrusion, a second one can grow and so on (d).

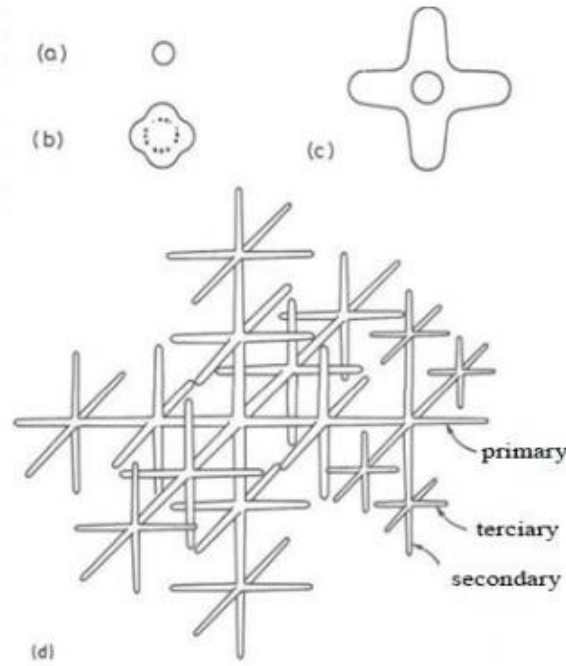


Figure 22: Dendritic growth during solidification. [9] [23]

The works previously carried out either by Luis Carlos Arias Garcia [22] who worked on the creation of the 3D printer, and by Mattis Muller [9] who worked on the design of an inductor for the electromagnetic induction heating system involved during extrusion, were performed with the premise that a thixotropic behaviour was desired, and this behaviour can only be achieved from globular structures.

Among the effective solutions is to apply a high shear velocity in the molten metal to be able to break the protrusions and therefore obtain solid particles of spherical shape in the liquid phase. The Figure 23 below, explicates how the shear stress at high velocity permits the obtention of the spherulite microstructure (e) thanks to the deformation ((c) & (d)) of the protrusion ((a) & (b)). [9]

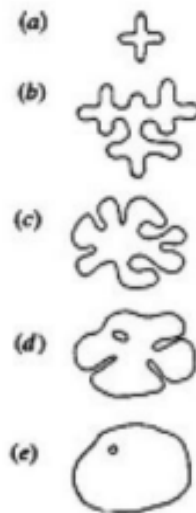


Figure 23: Evolution of the microstructure during solidification with a shear stress. [9] [22]

In practice, there are two ways to get this type of highly desired microstructure: [9]

1. From the molten metal or rheocasting process (Figure 24):

This option is hardly realisable in this project system case because breaking the dendritic microstructure in the liquid phase requires the application of a very high shear velocity along the whole extruder body and due to the complicated thermal gradient. In this case, three states coexist: solid, liquid and semisolid. [9]

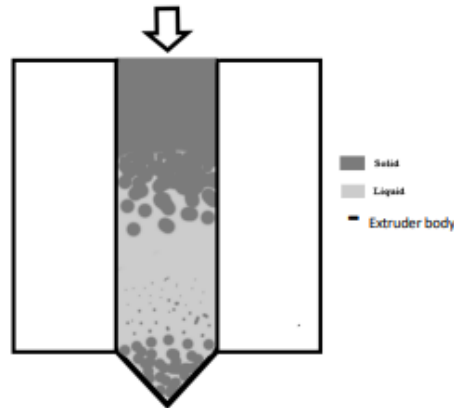


Figure 24: Microstructure along the extruder body in rheocasting. [9]

2. From the solid or thixotropic forming (Figure 25):

Its principle is heating a solid until the semi-solid state. One of its disadvantages is that if during the heating the core of the metal is still solid and the majority of the liquid is created at the surface, the forming will not be possible. Thus, it is very important to have a good homogenisation between the liquid and the solid. The globular shape of the solid, which is important to obtain a thixotropic behaviour, will have to be reached in previous rheocasting processes. Nevertheless, as the figure 25 shows, in thixotropic forming there are only the semi-solid state and the solid one. So, this way is a better option for the current application. [9]

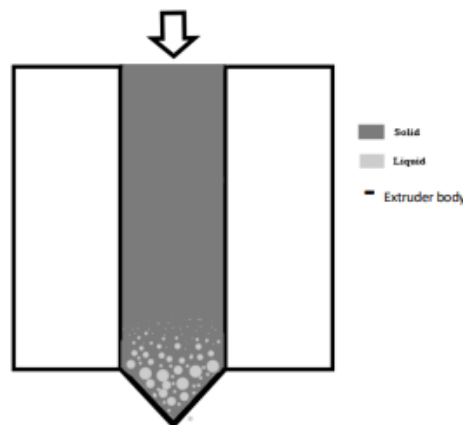


Figure 25: Microstructure along the extruder body in thixotropic case. [9]

## 3. Induction heating

### 3.1. Definition & Physical phenomenon

The objective of this section is to evaluate the theoretical aspects of electromagnetic induction heating. This technology was chosen as a heating system for the alloy to be extruded with the 3D printer for several reasons:

- A different option to resistance heating is required because of the higher melting temperature of the material to be extruded (Aluminium 357.0-F), unlike polymers. [9]
- The very low electrical resistivity of metals (0.00000440 ohm-cm for Al357.0-F), encourages the use of an induction heating system. [9]

Electromagnetic induction heating is one of the electrothermal techniques used to heat a determined material without direct contact with an electric power source, and its principle is dipping the part in a time-varying electromagnetic field, and to dissipate the energy entering the body in form of heat. It is distinguished from other techniques such as microwave and infrared by two things: [24]

- The electric frequency band used, that is to say by the penetration depth and the heating power densities obtained.
- The nature of the heated materials.

Indeed, it can be applied only to electrically conductive materials. In other words, electromagnetic induction heating is valid for materials with resistivity values included between  $10^{-8}$   $\Omega\cdot\text{m}$  (copper) and  $10^{-1}$   $\Omega\cdot\text{m}$  (melted glass), which corresponds to an electrical conductivity between 10 S/m and  $10^8$  S/m. The frequency band ranges from the order of 1 Hz (or maybe less) to a few megahertz which is equivalent to values between a few micrometres and a few centimetres for the penetration depths, and the surface power densities may reach higher  $10^5$  kW/m<sup>2</sup>. [24] The high-power densities involved make it possible to obtain very fast heating speeds. In addition, the special feature of generating heat directly inside the material gives many advantages compared to other standard heating methods, for instance, high yields, reducing heating times and the possibility of heating in a very local way. [25]

Induction heating systems are used principally in metallurgy and mechanics, like in heating before forming, fusion and some heat treatments. However, induction heating applications have emerged in other fields such as the food industry and chemistry (direct fusion of glasses and oxides) thanks to the evolution of electronics technologies and the appearance of faster switching components. These installations generate predominant magnetic fields near the inductor and power supply cables that are more important when the current passing through the inductor is higher. [26]

The table 2 below gives some examples of applications of induction heating:

Heating type	Frequency	Applications
penetrating	1 Hz to a few kHz (0,1 to 5 MHz for semiconductors)	Forge, fusion
superficial	10 to 500 kHz	Temper on the surface, brazing
film	10 to 1000 kHz	Welding of the tubes, thermal sealing

Table 2: Examples of applications of induction heating. [26]

The principle of this technology is based on different physical phenomena: [26]

1. A winding (inductor), that can take different shapes adapted to the geometry of the part to be heated, is traversed by a current at the desired frequency, thus, the creation of a magnetic field variable in time.
2. Creation of a current within the object thanks to the electromagnetic induction. This phenomenon occurs when a conductive element is immersed in a variable magnetic field.
3. Heating of the part due to the induced current. This is the Joule effect.

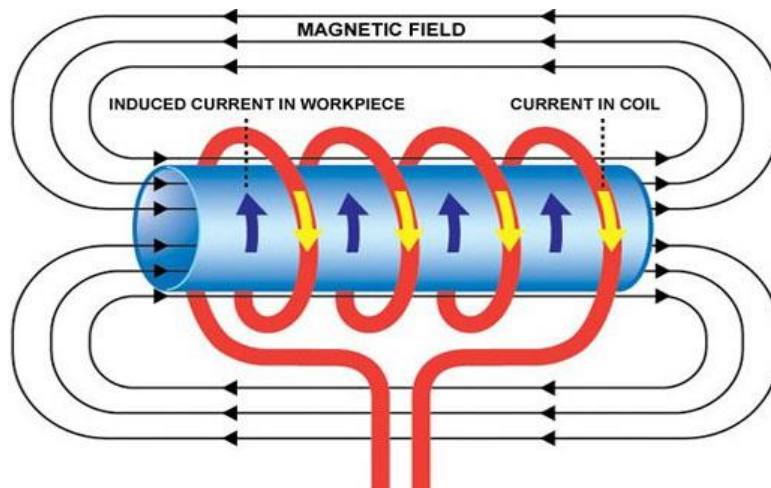


Figure 26: The principle of induction heating. [27]

## 3.2. Mathematical approach of the electromagnetic induction heating

### 3.2.1. Electromagnetic transfer between inductor and charge

The physics of this phenomenon is described by the Maxwell equations. An electric field (E) is created by the variation of the magnetic induction (B) applied to a material. If the material is an electrical conductor, the electric field (E) causes the creation of an electric current characterised by a density (J). [24]

The Maxwell equations makes it possible to quantify the various useful quantities which are solutions of the following mathematical expressions: [24]

- The relation between induction (B) and electric field (E):

$$\text{rot } \vec{E} = -\frac{\partial \vec{B}}{\partial t} + \text{rot}(\vec{v} \wedge \vec{B}) \quad (\text{Eq.3})$$

With:

- v: relative velocity of material displacement in relation to the induction
- For a slow-moving part, the rotational expression is zero or neglected.
- The relation between current density (J) and magnetic field (H), neglecting the displacement currents:

$$\text{rot } \vec{H} = \vec{J} \quad (\text{Eq.4})$$

- The relation between electric field (E) and current density (J):

$$\vec{J} = \sigma \vec{E} \quad (\text{Eq.5})$$

With  $\sigma=1/\rho_e$  the electrical conductivity of the material, and  $\rho_e$  is the resistivity of the material.

- The relation between magnetic field (H) and induction (B):

$$\vec{B} = \mu \vec{H} \quad (\text{Eq.6})$$

With  $\mu$  the magnetic permeability of the material.

Equations (Eq.4) and (Eq.6) permit the obtention of the repartition of the induced current. [24]

If the magnetic permeability is non-variable, by combining the mathematical expressions above, an interesting equation is obtained:

$$\frac{\partial \vec{B}}{\partial t} = \frac{1}{\mu \sigma} \Delta \vec{B} + \text{rot}(\vec{v} \wedge \vec{B}) \quad (\text{Eq.7})$$

Here,  $\Delta \vec{B}$  is the Laplacian of induction and it may be expressed by:

$$\Delta \vec{B} = j\omega \sigma \mu \vec{B} \quad (\text{Eq.8})$$

In this case, the variation of  $\mathbf{B}$  is sinusoidal with a frequency  $f$  and for immobile parts, with:

$$j^2 = -1 \quad (\text{Eq.9})$$

And the pulsation of  $\mathbf{B}$  is:

$$\omega = 2\pi f \quad (\text{Eq.10})$$

The spatial distribution of the induction can be found by the resolution of the equation (Eq.7) or (Eq.8), using the conditions at the limits of the load to be heated. [24]

However, analytical solutions can only be found for materials of constant magnetic permeability and simple cases such as plane, plate, cylinder or tube shapes or else numerical methods will be required to resolve these equations. [24]

### 3.2.2. Thermal effects

In electromagnetic induction heating cases, the material is heated by the Joule effect due to the influence of the induced electric current ( $I_x$ ). Indeed, 87% of the induced power is in the penetration depth  $p$ . Thus, it is possible to consider as a first approximation that the thermal source is localised in the surface area of thickness  $p$ . [24]

The heating of the material depends principally on three factors: [24]

- The propagation of heat in all the material.
- Exchanges with the environment of the part.
- The time during which power is applied.

The heated zone of the part constitutes the thermal penetration zone.

The study of the temperature evolution within the material is generally complex in such a way that it is possible to do it analytically only for simple cases. It is, therefore, necessary to proceed numerically for more complicated cases. [24] The famous heat equation below permits, using initial and boundary conditions, the calculation of the temperature distribution at each moment:

$$\rho c \left( \frac{\partial T}{\partial t} + v \text{ grad } T \right) = \text{div}(\lambda \text{ grad } T) + p_v \quad (\text{Eq.11})$$

With:

- $\rho$ : density.
- $c$ : specific heat capacity.
- $v$ : displacement velocity of the material.



- $\lambda$ : thermal conductivity.
- $p_v$ : volume density of electromagnetic power induced in the material.

The initial temperature condition is:

$$\mathbf{T}(\mathbf{x}, \mathbf{y}, \mathbf{z}, t) = T_0(\mathbf{x}, \mathbf{y}, \mathbf{z})$$

Surface temperature is set (this case is rare in induction heating):

$$\mathbf{T}_s = \mathbf{T}(\mathbf{x}, \mathbf{y}, \mathbf{z}, t)$$

A thermal flux is exchanged by convection with the atmosphere from the surface of the material, its mathematical expression is:

$$\varphi = h(T - T_a) = -\lambda \frac{dT}{dn} \quad (\text{Eq.12})$$

With:

- $h$ : convective exchange coefficient of the environment.
- $n$ : normal vector to the surface.

Unfortunately, the analytical resolution of these equations in the case of this research project is not possible because of the geometric complexity of the system to be heated, and because of the different material parameters to be taken into account. It was therefore necessary to use numerical finite element simulation to deal with the problem. This is what Mattis Muller [9] tried to do previously in their works using DEFORM software.

## 4. Experimental procedure

### 4.1. 3D printing machine

The project is part of the development of a printing machine (Figure 27) initially designed in a collaboration between the CIM Foundation and the Metal Forming Processes (PROCOMAME) research group, both belonging to the Universitat Politècnica de Catalunya (UPC).

The principle of operation is the extrusion of aluminium billets, placed inside the channel of the main body of the extruder, by the application of a pressure, thanks to a piston that can reach up to 700 bar. The nozzle, located in the lower part of the extruder is heated with an induction furnace YUELON. The aluminium alloy inside the nozzle is expected to heat up by conduction from the nozzle until reaching the semi-solid temperatures. Once the temperature is reached, the material is expected to come out of the nozzle and be deposited on the 3D printing platform which can move in all three directions of space and therefore print the designed part. [28]





Figure 27: The 3D printing machine and its components.

The main systems are: [28]

- Extruder and pressure system:

This part is composed by the extruder body and the nozzle (attached to the bottom of the extruder body by 8 bolts), both built on H-13 tool steel (Figure 28).



Figure 28: The extruder body, the nozzle, and the 8 bolts.

The pressure application system, which includes a hydraulic piston (Figure 29) and a pump (Figure 30), able to reach 700mbar. The piston is moved using a manual console (Figure 31). The maximum pressure to be applied by the pump is selected in the pressure regulator and the manometer allows pressure measurement (Figure 32).



Figure 29: The hydraulic piston.



Figure 30: The pump.



Figure 31: The manual console.

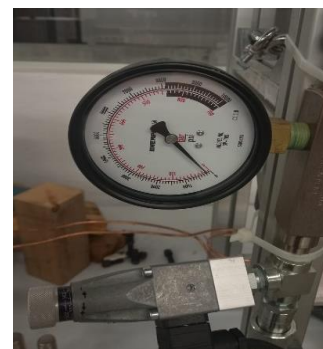


Figure 32: The pressure regulator and the manometer.

- XYZ system for printing:

In the printer, the XYZ movement is conferred to the building platform (Figure 33) and there is an electronic board for the control of the process (Figure 34):



Figure 33: The building platform.



Figure 34: The electronic board for the control of the process.

- Heating system (Figure 35):



Figure 35: The heating system.

In order to realise the different experiences, an YUELON model HF15-A inductor with 7KW input will be used (Figure 36). A water-cooling system is connected to the inductor to avoid any unwanted increase in temperature (Figure 37).



Figure 36: YUELON model HF15-A inductor.



Figure 37: The water-cooling system.

This inductor requires a Proportional Integral Derivative (PID) controller to control and fix the temperature (Figure 38). The line above shows the temperature read by the thermocouple and that below is the temperature set by the user. To reach the desired temperature, the controller PID will turn on and stop the induction oven in such a way that the selected temperature value is maintained.



Figure 38: PID Eurotherm serie 3204.

The steps to use the machine are: [28]

1. Activate the hydraulic system and 3D base with the electronic board.
2. Move up and down the piston with the switch on the manual console.
3. Select the desired pressure by turning the pressure controller on the side of the extrusion system.
4. Select the work temperature of the induction furnace controller that is connected to a thermocouple attached to the nozzle.
5. Turn on the induction furnace to heat up the nozzle. But before doing that, it is very important to make sure that the refrigeration channels are open, and water is running in order to protect the induction furnace from burning when the temperature reaches very high values.
6. Once the desired temperature is reached, the extrusion can start. It is possible to retract and extend the piston during the whole process to hit the billets many times, and to variate the pressure in conjunction with using the pressure controller.

## 4.2. Heating trials

The purpose of this step was to perform the first heating tests on the new nozzle redesigned after the one analysed in a previous work by Mattis Muller [9] and used for initials extrusion trials during the development of the 3D printer. The new nozzle required a new coil which was designed at the beginning of this project. The design of the coil is detailed in the “Results and Discussion” section.

After the design process of the coil, it was constructed, and some initial heating trials were performed. These thermal tests were done only on the nozzle without being mounted to the body of the printer to be able to evaluate the thermal profile of the interior wall. Technically, this will be impractical if the nozzle is attached to the 3D printing system because in this case, it would not be possible to fix thermocouples inside. The temperature profile was thus evaluated only in the inner part of the nozzle and in one point outside because it was complicated to connect more than one thermocouple to the outer wall. Therefore, three thermocouples were positioned inside as Figure 39 shows.

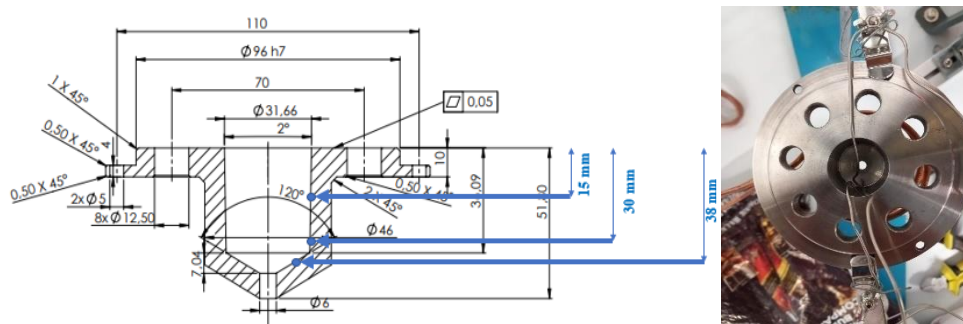


Figure 39: The positioning of the thermocouples inside the nozzle.

The distance left vertically (z-axis) between the nozzle and the coil is equal to 20 mm. It corresponds to the sum of the height of the screw head (5mm) and the safety distance



that must be left between the coil and the screws (15mm) so as not to damage them due to the magnetic field that will be created and the thermal effects.

The thermocouples (type K) that were attached to the nozzle were connected to a PicoTech TC-08 thermocouple itself connected to the software Picolog which allows to trace the evolution curves of the thermal profiles for the different thermocouples (Figure 40).



Figure 40: TC-08 thermocouple data logger.

The setup of the heating trials is illustrated in Figure 41 below:

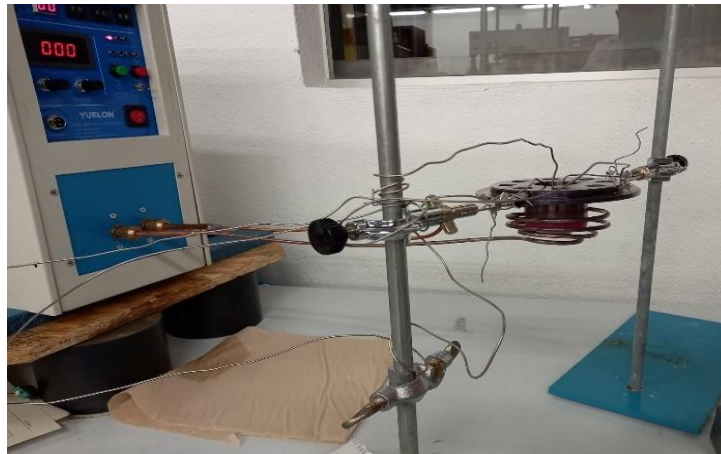


Figure 41: Setting up the experiment.

This setup was used to check the coil designed in the first stages of the project, as well as modifications of the coil aiming at a better control of the temperature profile, according to the results of the extrusion trials

### 4.3. Extrusion trials

Different extrusion trials were performed to check the effect of the different heating setups, which included modifications of the coil. In this trials, aluminium samples (Figure 42) were introduced in the body of the extruder and heated for 10min before applying pressure to the system through the piston. Pressure was gradually increased during the trials and maximum pressure applied was 600mbar.



Figure 42: Aluminium samples.

### 4.4. Samples preparation

After the extrusion trials, the material which has gone through the nozzle was characterized microstructurally to check whether the microstructure exhibited a globular morphology (typical of thixotropic alloys) or dendritic features, an indication of melting which is not desirable. Metallographic preparation of the samples included different steps, is described next.

#### 4.4.1. The cut of the sample

The Al357.0-F sample was cut with a metal cutter using a diamond disc. To put it simple, the general scheme of the sections made, and the different planes chosen to make them is schematized in Figure 43 below:

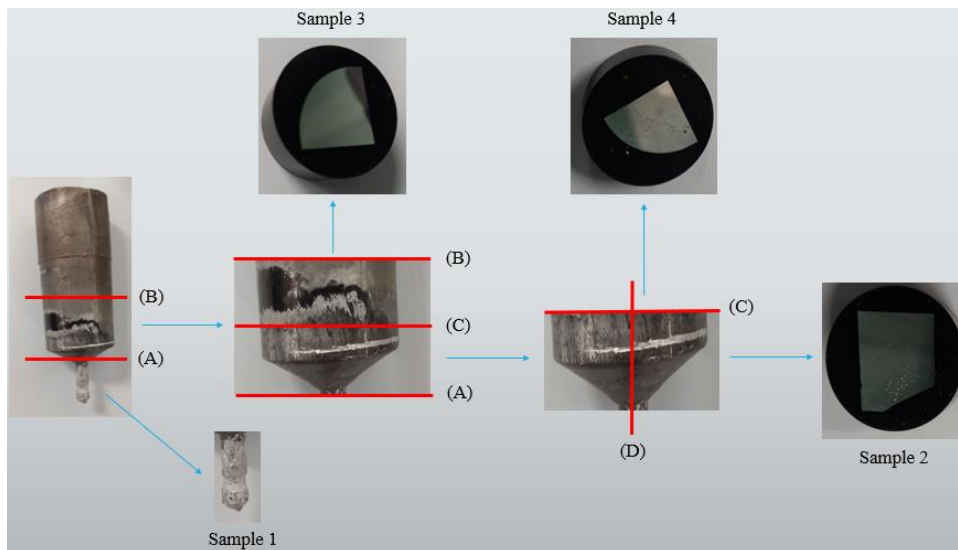


Figure 43: the general scheme of the cutes made.

These 4 samples were therefore coated, polished and analysed.

#### 4.4.2. Mounting

The 4 samples were small enough to be placed directly into the hot coating machine “Struers LaboPress-3”(Figure 44). Each sample must be placed in the channel of the machine while taking care that the surface to be observed is well placed towards the bottom. Then, hot resin is poured, and the coating is launched (it takes more or less 10 minutes).



Figure 44: Struers LaboPress-3 hot coating machine.

#### 4.4.3. Polishing

This was the most delicate step in the whole process of metallographic work because the quality of the images that were seen later in microscopes, including OM and SEM, depended heavily on it. It must therefore be done with caution and following the protocol agreed for polishing aluminium and its alloys. The samples were polished using a “Struers LaboPol-5” polisher (Figure 45) which is a machine made up of a turntable on which is deposited a polishing disc with the desired grain. An open water tap for the entire polishing time overhangs the tray, but not when diamond disks are used.

With regard to the principle of polishing: larger-grained discs are used first, and then the size of the grains is reduced as you go. The aim is to obtain a perfectly smooth and flat sample surface. One of the difficulties is keeping only one facet by holding the sample in hand.



Figure 45: “Struers LaboPol-5” polisher.



The procedure can be summarised as follows:

1. Use discs from 240 to 1200 grains using water in a continuous way.
2. Use diamond discs that contain much finer particles without using water but using diamond solutions (9 $\mu$ , 6 $\mu$ , 3 $\mu$  and 1 $\mu$ ).
3. A vibratory polisher “Buehler Vibromet 2” can be used to ameliorate more the surface state (Figure 46). It requires a colloidal silica solution.



Figure 46: Buehler Vibromet 2 vibratory polisher.

4. An ultrasonic cleaner can also be used (Figure 47).



Figure 47: Ultrasonic cleaner.

5. Finally, additional fieldwork of stripping needs to be undertaken. A 10 second chemical attack with a solution of hydrofluoric acid was therefore carried out for the 4 samples, and the concentration of hydrofluoric acid taken in this case is 3%. However, this compound is extremely toxic and corrosive, and it must be handled with important precautions such as the use of gloves, blouse, protective glasses and ventilation. It should also be stored in plastic test tubes and certainly not in glass tubes because HF is one of the few known liquids that can dissolve glass.

#### 4.5. Final heating and extrusion trials

Towards the end of this research project, the good news was the acquisition of a new welder machine type "SR80 Universal" purchased from the UK (Figure 48). It was very useful because it permitted to weld thermocouples in precise points on the nozzle, which was not possible in the first experiments (Part of Heating trials) where thermocouples were very difficult to attach to the metal.

This welder is based on the principle of capacitance discharge, and it is manufactured for use in fine wire welds applications, in particular the welding of thermocouples. Its accessories are: pliers, power cable, magnifier, 2mm allen key, red filter, spare carbons (2), footwitch, argon hose and black lead with croc clip. [29]

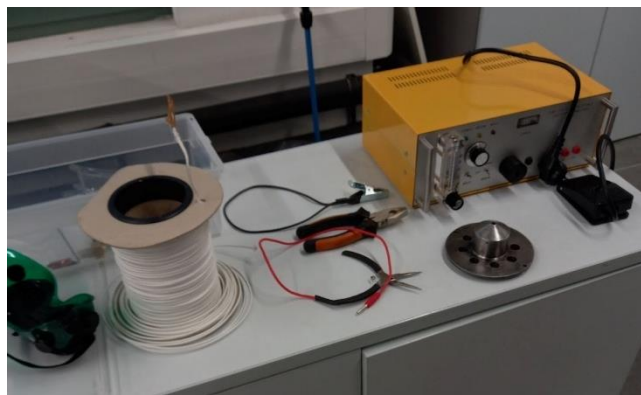


Figure 48: The SR-80 Universal Welder and its accessories.

The purpose of the next step was to do a thermal heating test using the new welder to fix 4 thermocouples inside the nozzle to study the thermal gradient. Another one was welded on the exterior surface. As for the first heat experiments, the reasoning followed was to, first, perform these thermal tests only on the nozzle without being mounted to the body of the printer to be able to evaluate the thermal profile of the interior wall. The advantage this time is that thanks to the welder, it was possible to better control the positioning of each thermocouple as well as to put more than in the first case (Figure 49). In addition, a thermal insulation wool was installed above the nozzle to limit the effect of the convection of the ambient air on the thermal profile inside (Figure 50).



Figure 49: Four 4 thermocouples welded inside the nozzle.

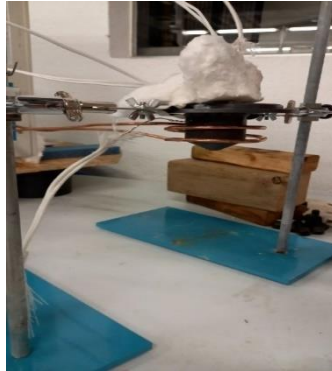


Figure 50: Thermal insulation wool installed above the nozzle.

## 5. Results and discussion

### 5.1. Coil conception

The first part of this research internship consists of the design and manufacturing of the coil that will be used in the induction heating of the AM system. The previous research works done by Mattis Muller [9] suggested the use of a 3-spiral coil, with an internal diameter centre to centre equal to 130 mm, and an inter-spire distance centre to centre equal to 16mm.



Figure 51: The old extrusion head. [9]

However, the old model of the 3D printer nozzle shown in Figure 51 above had several problems with the flow of the alloy inside and with heat transfer. A new model was then developed by Sergio Alberto Elizalde Huitron (Figure 52).

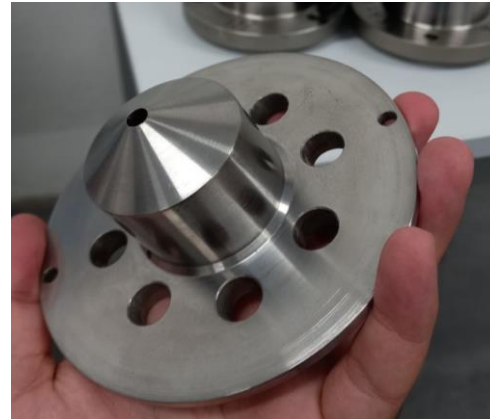
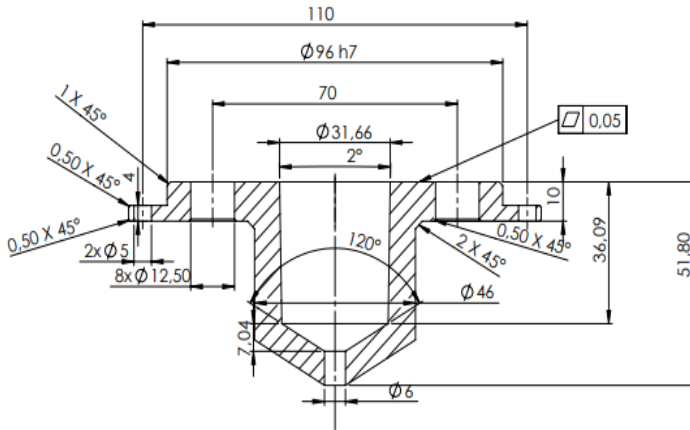


Figure 52: The new model of the nozzle.

The geometry of the nozzle has completely changed so new dimensions was used for the inductor to be created in this new case:

- 4 spires.
- Diameter of the copper wire  $d=4\text{mm}$ .
- Inter-spire distance centre to centre  $a=10\text{mm}$ .
- Distance between the outer wall of the nozzle and the outer wall of the coil  $l=10\text{ mm}$ .

The design of the coil which accomplishes the requirements is depicted in Figure 53.

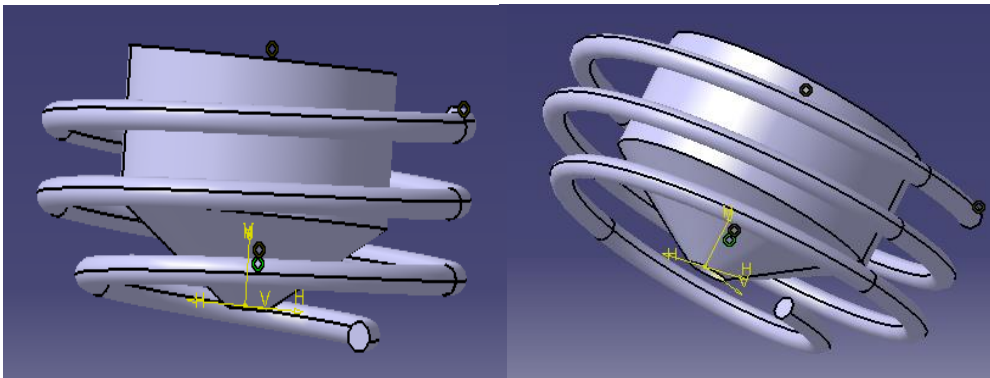


Figure 53: 3D model of the nozzle inside the coil.

The next step was manufacturing a part which was used as a die to give the desired spiral coil shape to the copper wire, and thus, use it as an inductor for the printing system. To do so, a digital 3D model was made on the CATIA software (Figure 54). It has been designed and adapted from the dimensions of the extrusion nozzle and the coil to be manufactured so that the copper wire can take the shape of the desired coil.

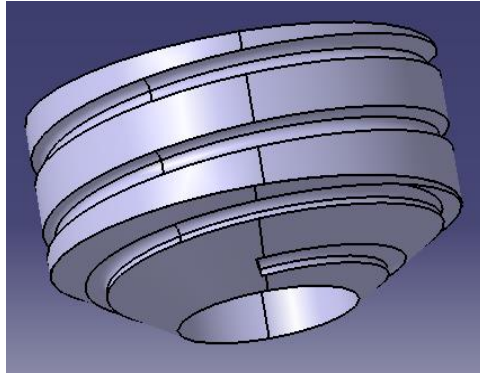


Figure 54: 3D model of the part printed.

A quick and easy way to make this part was to use the additive manufacturing of polymer materials technology. A 3D printer was therefore used, and the PLA (Polylactic acid), a very used polymer in AM, was chosen as a raw material for the simple reasons of its availability in large quantities in the laboratory, its simplicity of implementation and its low melting temperature (175°C) (Figure55).

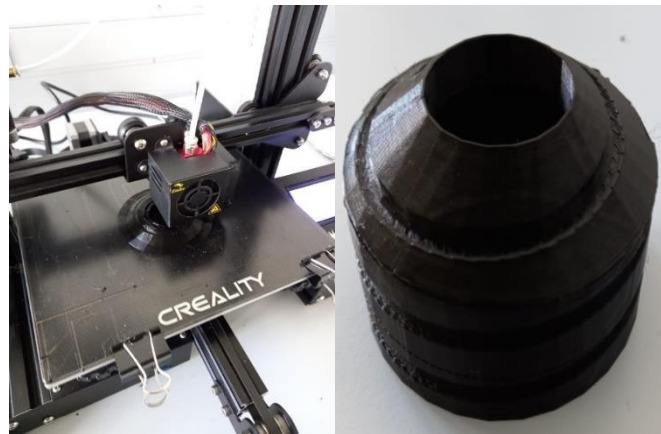


Figure 55: The polymer 3D printer used (left) and the PLA part printed (right).

The next step was to wrap the copper wire around the PLA piece to give it the shape of the copper coil. As shown in Figure 56, the final result was very satisfactory because the dimensions of the manufactured coil fit perfectly with those of the extruder.



Figure 56: The nozzle inside the coil.



## 5.2. Heat experiments

### 5.2.1. Experiment 1

The main purpose of this first experiment was to evaluate the thermal profile within the interior wall of the nozzle, and subsequently quantify the temperature value taken by the thermocouple fixed at the outside point of the part. This allowed in the next steps of the project to control the thermal profile inside only through the outer thermocouple since it was practically and technically not possible, during extrusion, to put and fix thermocouples inside. In this experience, the PID controller was connected to the thermocouple fixed in the inferior part inside the nozzle (thermocouple closest to the extruder outlet as indicated in Figure 57), and it was programmed at a temperature of 580 °C which corresponds to the ideal temperature for working with Al357.0-F in its thixotropic state.

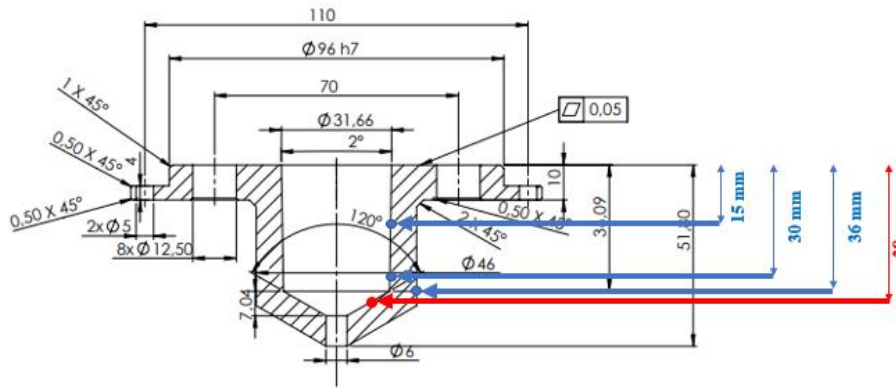


Figure 57: The thermocouple closest to the extruder outlet.

The first successful test has given the thermal profile shown in Figure 58 below:

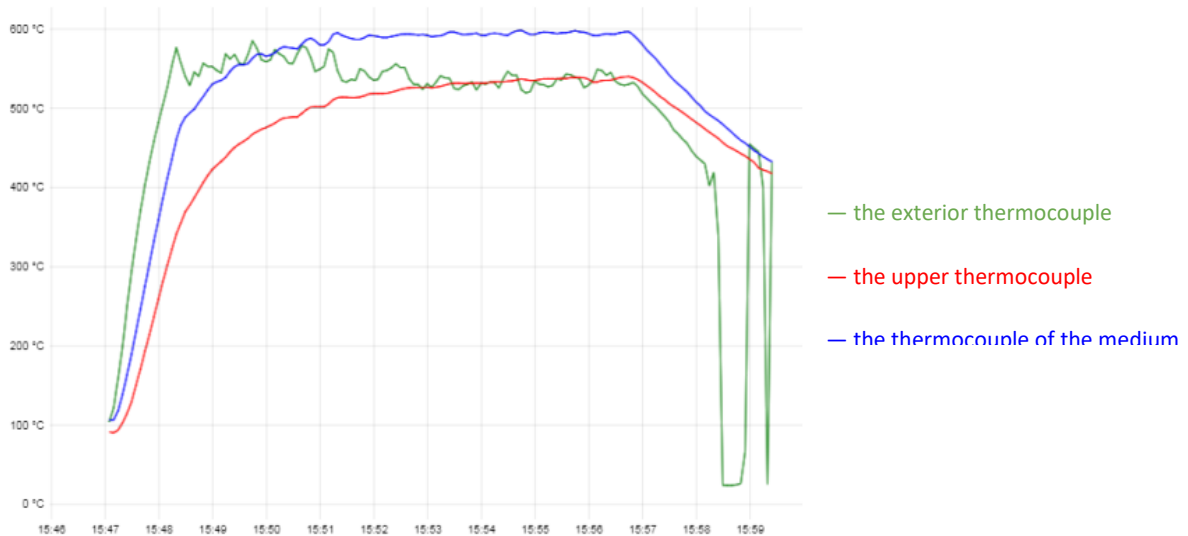


Figure 58: The thermal profile of the first heat experiment.

Two main conclusions that can be drawn from this curve above:

1. The green curve shows that the temperature recorded at the outer point is about 540 degrees. It was, therefore, possible to consider, during extrusion experiments, the setting of a temperature of 540 degrees outside which would correspond to the temperature of the semi-solid state inside the nozzle and hence the alloy inside (about 580 degrees). This was verified experimentally during the experiment 2.
2. The thermal gradient between the two furthest measuring points (thermocouples) of this experiment is about 60 degrees. This could be explained by the temperature profile generated based on the induction parameters, as well as the convection movements generated by the ambient air in the laboratory, by the thermal conduction in the nozzle itself, and by the temperature differences between the air and the heated part.

### 5.2.2. Experiment 2

What changed in this experiment compared to the previous one is that this time the thermocouple connected to the PID controller was the one fixed to the outer surface of the nozzle, so the imposed temperature was 540 degrees. Figure 59 below shows the results obtained:

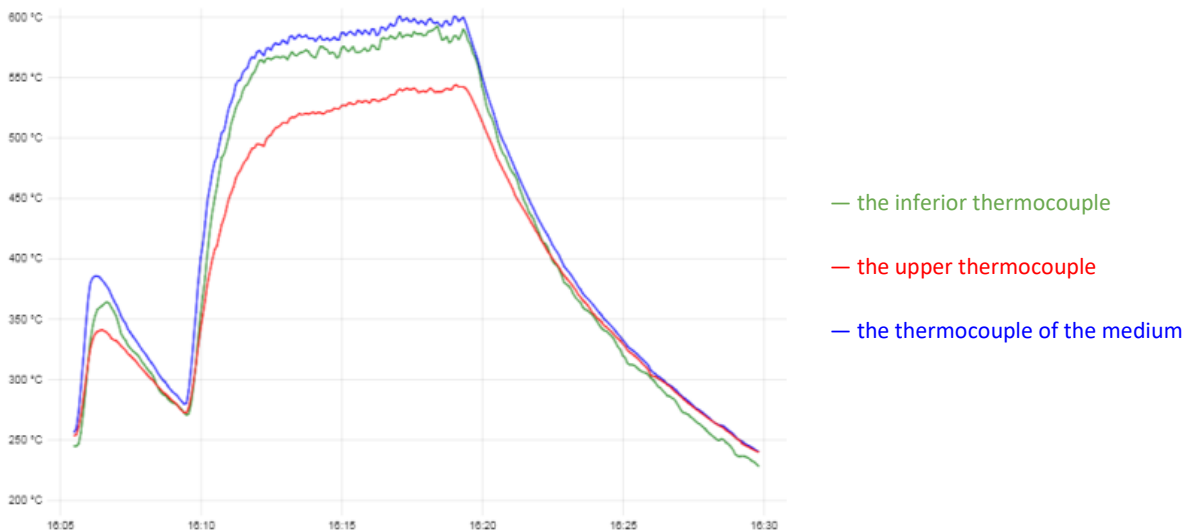


Figure 59: The thermal profile of the second heat experiment.

The green curve obtained confirms that a temperature value fixed at 540 degrees with the PID controller in the outside surface of the nozzle corresponds to 580 degrees at the point where the lower thermocouple is fixed inside (the point closest to the output of the nozzle). On the other hand, the temperature variations for the upper and middle

thermocouples are almost identical in the case of the preceding experiment (blue and red curves above). It is also remarkable that, in both experiments, the central measuring point always takes the highest temperature values (blue curve). This can be explained by the fact that the inductor coil creates its most important magnetic field in this area where the temperature is therefore maximum.

### 5.3. Extrusion experiments

In the following (experiment 1 of extrusion), the basis of the process was to make the hypothesis that the fixing of a temperature of 540 degrees at the external point of the nozzle would give an internal thermal profile of 580 degrees, which corresponds well to the temperature interval of the semi-solid state of the aluminium alloy.

To fully understand the process of extrusion experiments, it was necessary to present the general principle of operation of the 3D printer with its different components and their roles (Part of 3D printing machine).

#### 5.3.1. Experiment 1

In order to start the machine and perform extrusion tests, the nozzle must be mounted at the bottom of the printer. Then, following the experimental protocol described above, the first extrusion experiment was launched by imposing a temperature of 540 degrees with the PID controller, this with an intermediate of a thermocouple fixed on the same external point of the metal nozzle same as in experiments 1 & 2. The security distance of 20mm explained before (Part of Heating trials) was left between the nozzle and the coil. The thermal profile was not recorded because the only thermocouple on the outside was linked to the induction furnace controller.

As shown in Figure 60, part of the alloy was extruded with this system for the first time in this major research project. In the following, the nozzle was disassembled to remove the remaining aluminium alloy sample inside the channel machined in the main body of the extruder. Then, the extruded part of the material, as well as the part left inside was cut, prepared and analysed by OM and SEM.





Figure 60: Experiment 1 of extrusion.

To do so, the sample in Figure 61 has been mounted, polished and finally analysed.

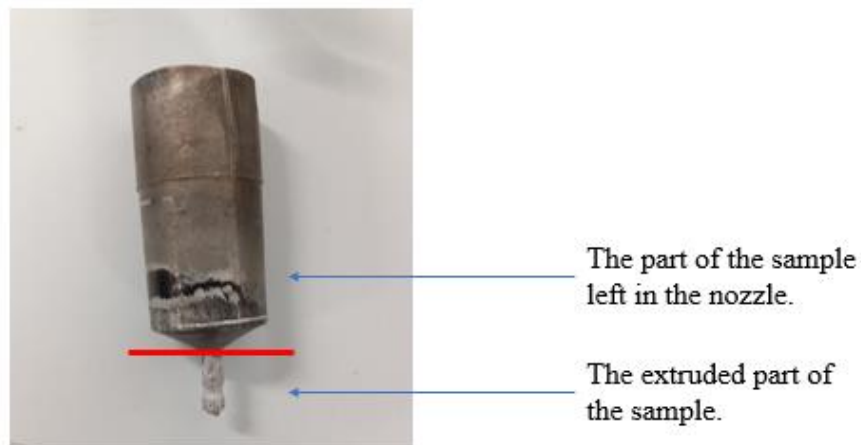


Figure 61: The sample to analyse.

### 5.3.2 Samples analysis

Once all the samples were polished, they were observed first in the optical microscope and later in the SEM. This made it possible to highlight the scratches to eliminate, and also the non-planarity of the surface. By repolishing samples that contained defects, the following results were obtained:

- **Sample 1**

The Figure 62 illustrates the three observation points where the analysis was done. The images obtained with the OM are shown in Figure 63, Figure 64 and Figure 65.

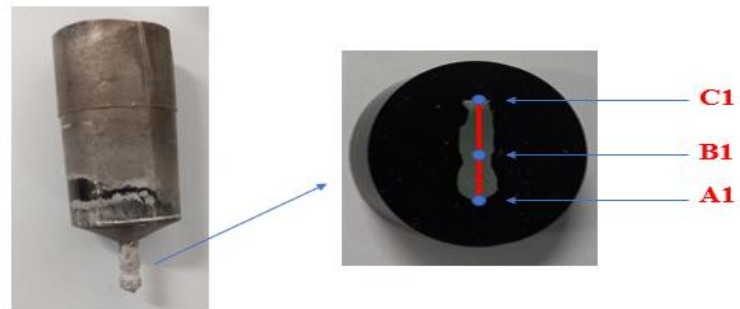


Figure 62: The three observation points A1, B1 and C1 in sample 1.

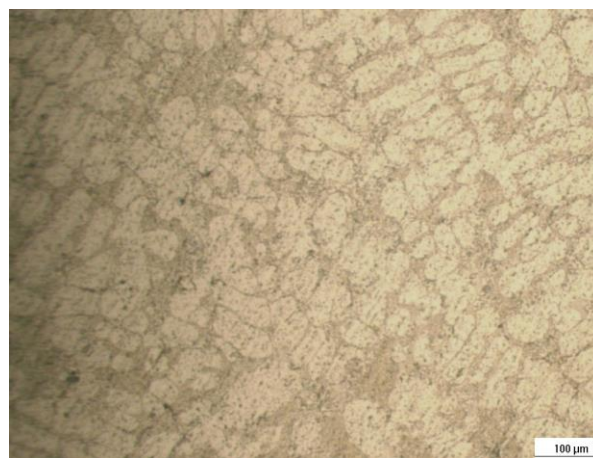


Figure 63: Point A1 observed with the au OM.



Figure 64: Point B1 observed with the au OM.

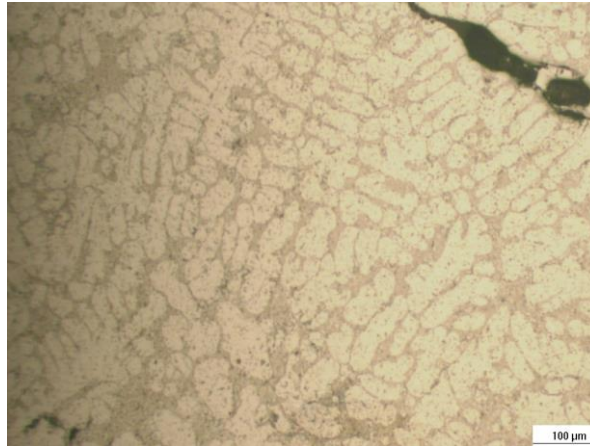


Figure 65: Point C1 observed with the au OM.

The images obtained with the OM have permitted to identify the presence of a dendritic structure throughout the part of the alloy that came out of the nozzle (sample1). This means that, unfortunately, this zone was melted during the extrusion experiment, so globular microstructure which promotes the thixotropic behaviour is lost during the heating process.

To verify the results obtained by optical microscopy, a SEM analysis was performed. This was done within the “Escuela Politécnica Superior de Ingeniería de Vilanova I la Geltrú” (Polytechnic School of Engineering of Vilanova I la Geltrú) as part of a collaboration with the host entity of this research internship the “Escuela de Ingeniería de Barcelona Este” (Barcelona East School of Engineering), both belonging to the “Universitat Politècnica de Catalunya”.

The images obtained with SEM confirm the presence of a dendritic structure throughout the sample 1, without any significant variation of the form or the size. However, given the complexity of the equipment of this type of microscope, it was very difficult to identify exactly where the images were taken. An example of images obtained is in Figure 66 as follows:

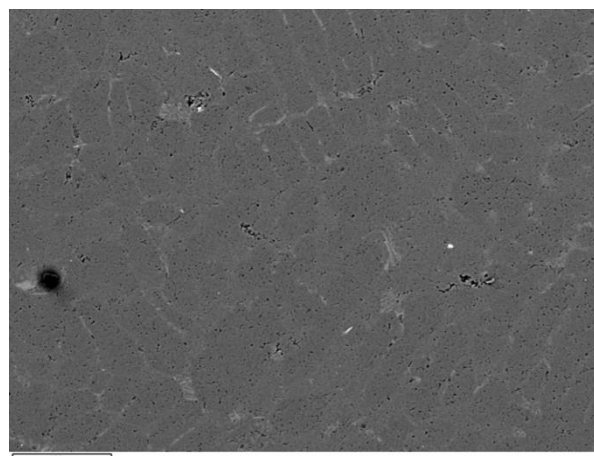


Figure 66: An example of images obtained with the SEM.

For this same area, a chemical composition analysis was performed (Figure 67 & Table 3).

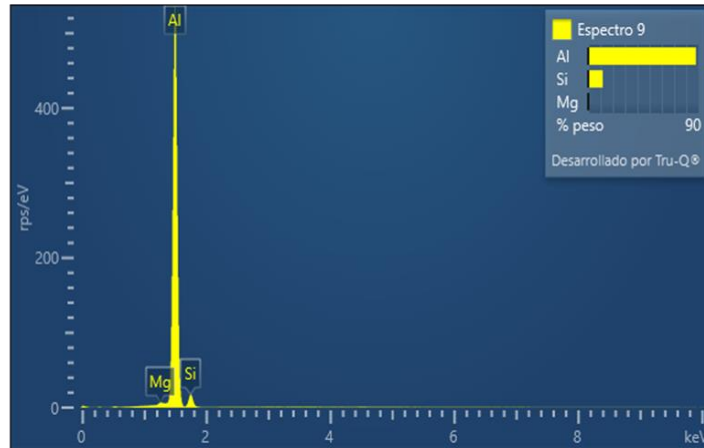


Figure 67: Spectrum of the area in Figure 66.

Spectrum	Weight %	Atomic %
Mg	0,40	0,45
Al	87,76	88,13
Si	11,83	11,42
Total	100,00	100,00

Table 3: Chemical composition of the area in Figure 66.

In the following, sample 2 was, in turn, analysed with the OM to see if the non-extruded Al357.0-F zone contains a granular structure which means that the material did not melt and kept the original microstructure.

- **Sample 2**

The methodology for this sample was the same as for sample 1. Several images were taken with the optical microscope following the scheme represented in Figure 68:

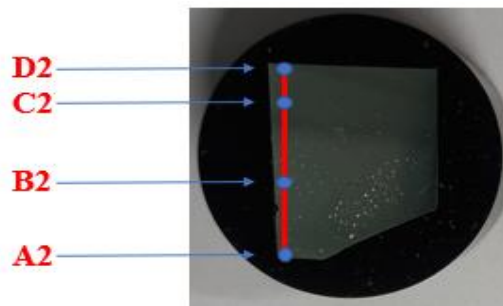


Figure 68: The four observation points A2, B2, C2 and D2 in sample 2.

The images obtained with the OM are shown in Figure 69, Figure 70, Figure 71 and Figure 72.

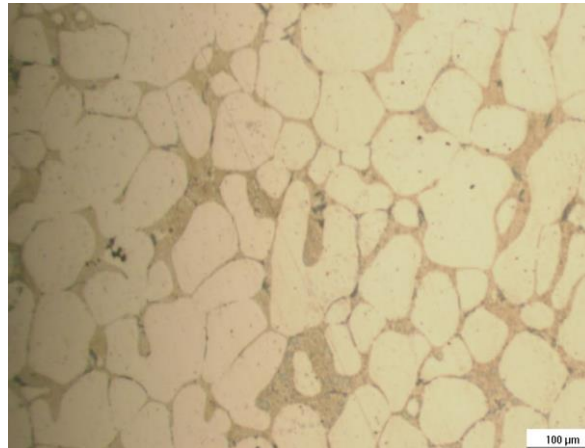


Figure 69: Point A2 observed with the au OM.

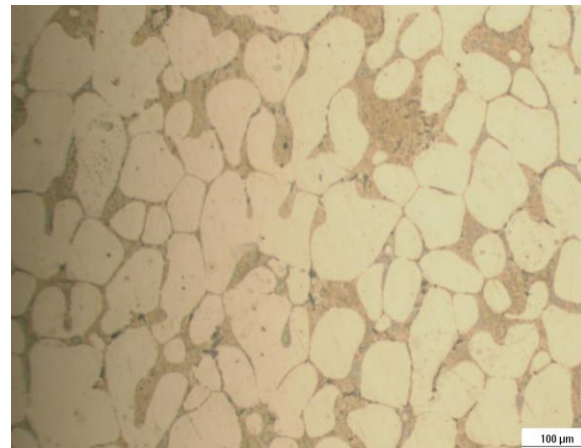


Figure 70: Point B2 observed with the au OM.

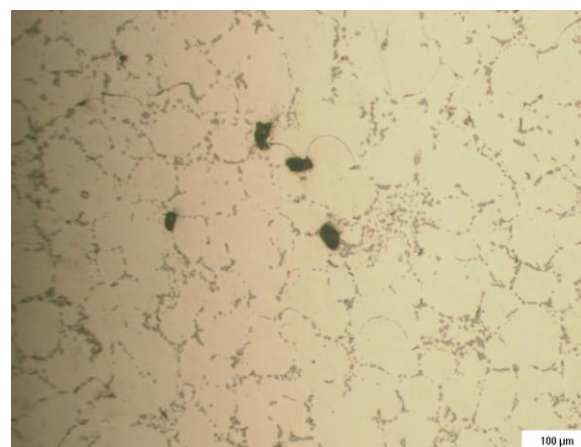


Figure 71: Point C2 observed with the au OM.



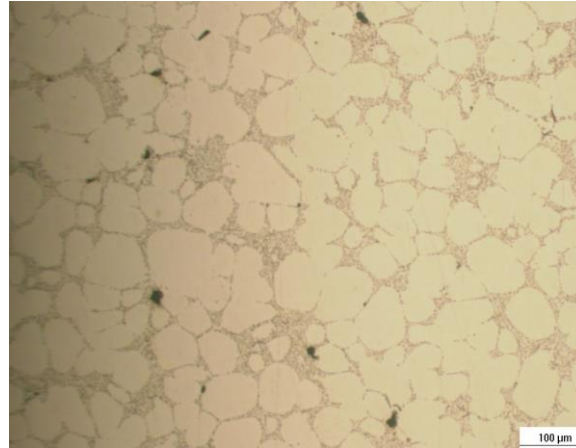


Figure 72: Point D2 observed with the au OM.

The results obtained are more or less homogeneous over the whole sample: the microstructure is granular and there are no dendrites, which means that the Aluminium 357.0-F alloy did not melt inside the nozzle during the experiment. Nevertheless, in the vicinity of point C2 (Figure 71), silicon precipitation was observed (Figure 73).

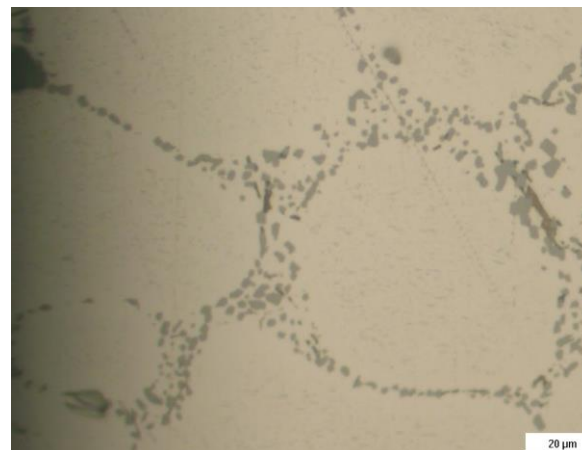


Figure 73: Silicon precipitation in point C2 observed with the au OM (x50).

This can be explained by the fact that this area has undergone the largest temperature increase of the whole sample as it corresponds to the area where the magnetic field created by the coil was maximum.

The SEM analysis also confirms that the structure is granular and that there are no dendrites in sample 2, an example of images obtained is in Figure 74 as follows:

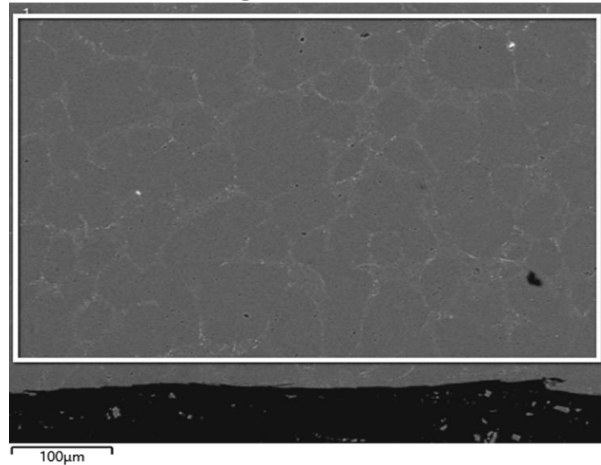


Figure 74: An example of images obtained with the SEM.

For this same area, a chemical composition analysis was performed (Figure 75 & Table 4).

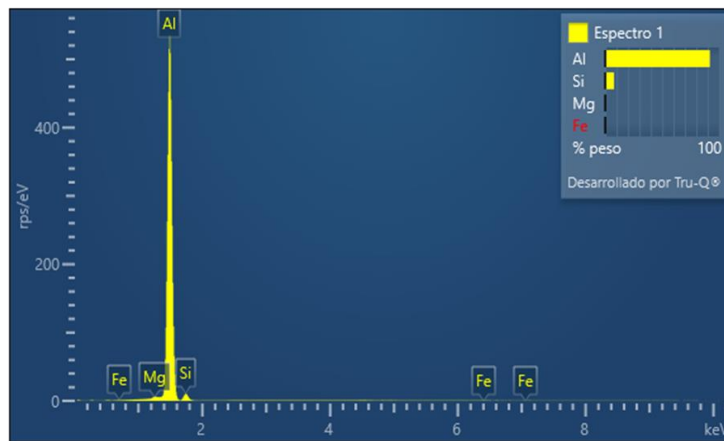


Figure 75: Spectrum of the area in Figure 74.

Spectrum	Weight %	Atomic %
Mg	0,33	0,37
Al	91,90	92,20
Si	7,65	7,37
Fe	0,12	0,06
Total	100,00	100,00

Table 4: Chemical composition of the area in Figure 74.

To prove that the precipitates shown in Figure 71 and Figure 73 are silicon, a chemical composition analysis was performed for the same area with the MES (Figure 76).

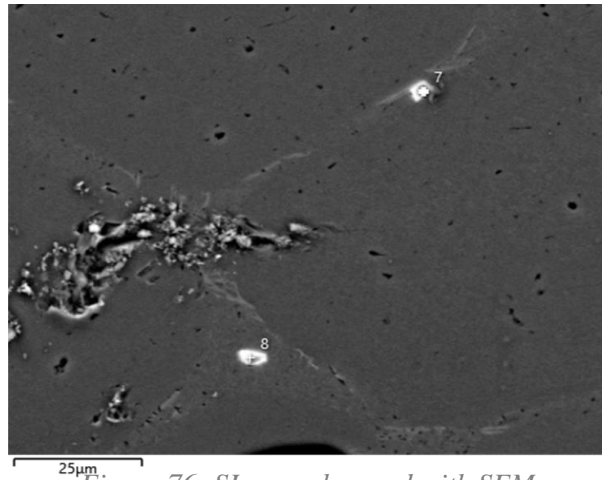


Figure 76: SI zone observed with SEM.

For this same area, a chemical composition analysis was performed (Figure 77 & Table 5).

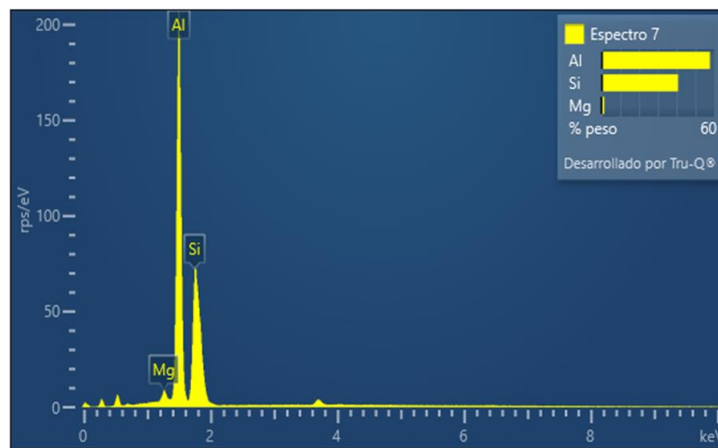


Figure 77: Spectrum of the area in Figure 76.

Spectrum	Weight %	Atomic %
Mg	1,55	1,74
Al	57,69	58,53
Si	40,76	39,73
Total	100,00	100,00

Table 5: Chemical composition of the area in Figure 76.

- **Average grain size calculations for sample 2**

To get an idea of the evolution of the grain size in this sample, calculations using the intercept method were made. These rough calculations show that the further away from



the nozzle outlet (point 1) the smaller the size of the grain. Thus, it can be concluded that the bottom has been longer at higher temperatures and there has been more grain growth. These calculations can be resumed in the figure 78 below:

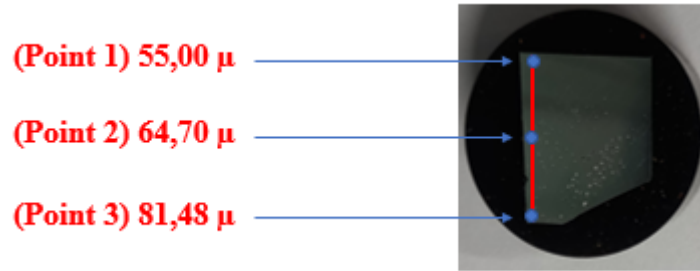


Figure 78: Average grain size calculations for sample 2.

Here, the intercept method which is a simple technique was used to estimate the average grain size and its evolution through the sample (Figure 79, Figure 80 & Figure 81).

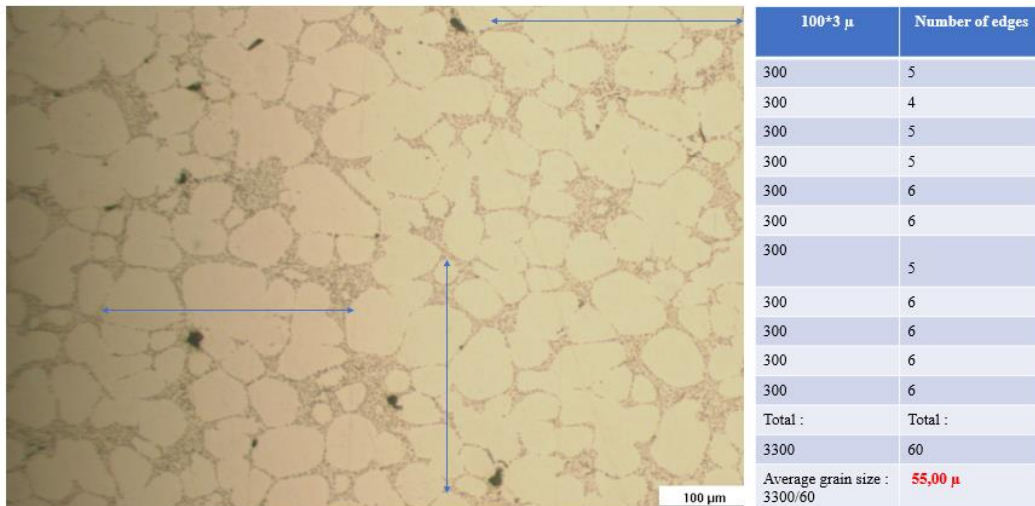


Figure 79: Calculations for point 1.

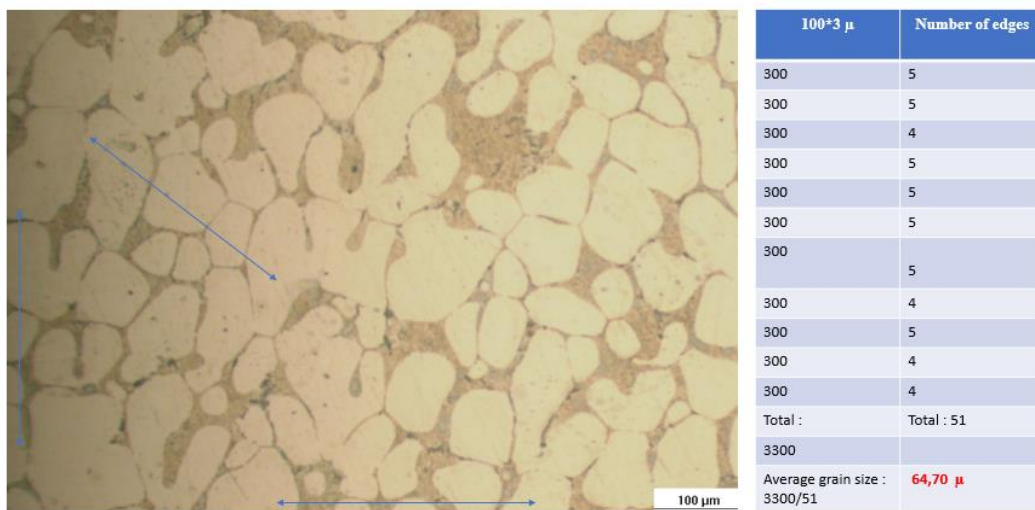


Figure 80: Calculations for point 2.

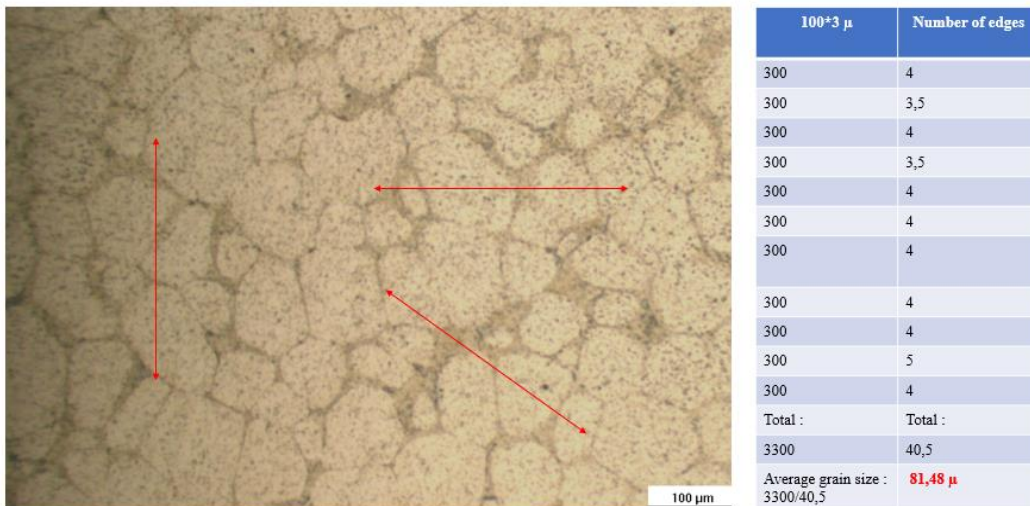


Figure 81: Calculations for point 3.

- **Sample 3 & 4**

Samples 3 and 4 (Figure 43) were also analysed with an optical microscope to see if the structure in these two areas is granular, and to verify if there is something strange in the microstructure. So, looking at different points in both directions of space, it was found that the entire microstructure contained grains and there was no particular precipitation or dendrites or anything else.

Among the images obtained (Figure 82 & Figure 83):

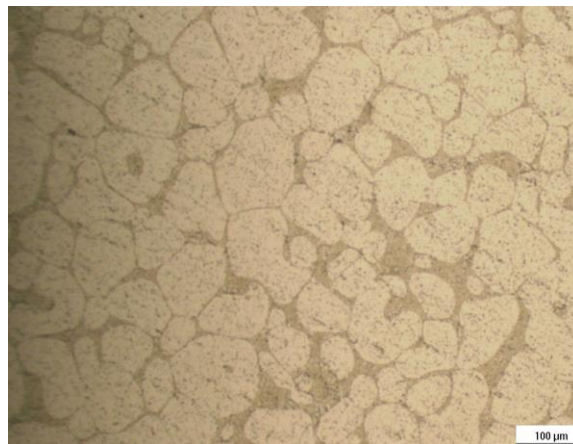


Figure 82: An example of images obtained with the OM for sample 4.

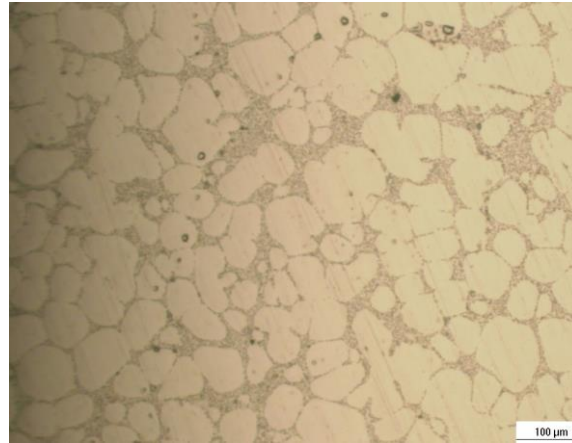


Figure 83: An example of images obtained with the OM for sample 3.

To conclude, it is clear that only the part of the alloy released from the nozzle during extrusion was melted because it is only there where there is a dendritic structure (temperature exceeded 580 degrees). The inner zone was as desired in the semi-solid state since it contains no dendrite but only grains. This problem of melting of the material at the outlet of the nozzle is due to the design of the coil and consequently to the high thermal load, the temperature of which is expected to exceed 580 degrees which characterises the semi-solid state.

For that reason, the solution was to eliminate the fourth (bottom) spiral of the coil and work with only three and evaluate experimentally whether this would create a sufficient magnetic field to heat the material to be extruded up to 580 degrees. The assumption taken in the experiment 2 of heating, which says that the fixing of a temperature of 540 degrees at the external point of the nozzle would give an internal thermal profile of 580 degrees, was maintained for this new case of 3-spiral coil.

### 5.3.3. Experiment 2

The parameters and settings for this second extrusion attempt were exactly the same as in the first experiment (the part of Experiment 1 of extrusion). The only thing that changed is the geometry of the coil (Figure 84) as well as the safety distance left between the top spiral and the 8 screws of the nozzle: 7 mm instead of 15 mm. The reason why this safety distance reduction decision was made is that even by eliminating a spiral to the old coil, a significant part of the latter remains below the nozzle outlet, which would probably have affected the outgoing material exactly like what happened before.



Figure 84: New coil of 3 spirals.

During the experiment, the new geometry of the coil greatly affected the magnetic field created and consequently the thermal profile in the interior of the nozzle had to change (increase in temperature values to more than 580 degrees because the nozzle has taken on a strong red colour). This made it impossible to control internal temperatures, which caused the fusion of the extruded alloy and thus the creation of a dendritic microstructure as shown in Figure 85 below.

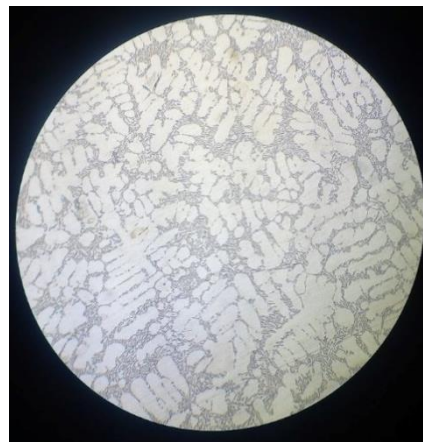


Figure 85: Dendritic microstructure in the second extrusion experiment.

Since the only way forward to try to extrude the alloy in a semi-solid state is to do experimental testing, the new idea is to eliminate another spiral from the coil and see how the nozzle and the material inside will react to the new magnetic field.

#### 5.4. New heating tests & the third extrusion experiment

In a first time, the thermal profile within the interior wall of the nozzle was evaluated, and subsequently the temperature value taken by the thermocouple welded at the outside point of the part was quantified. Following the same logic as in the first two heat experiments (part of Heat experiments), this has permitted later controlling the thermal profile inside only through the outer thermocouple. The PID controller was connected

to the thermocouple fixed in the superior part inside the nozzle (the farthest one from the extruder outlet). The methodology followed was to gradually increase the temperature value imposed by the PID controller on the thermocouple connected to it (the upper) until the thermal profile inside the nozzle was more or less close to the 580 degrees desired. The value taken by the outer thermocouple was 315 degrees and by the PID controller was 535 degrees. It has to be taken into consideration that for this experience, the lower spiral of the inductor was removed because the previous experience showed melting (higher temperature) at the exit of the nozzle.

The thermal profile founded is shown in Figure 86 bellow:

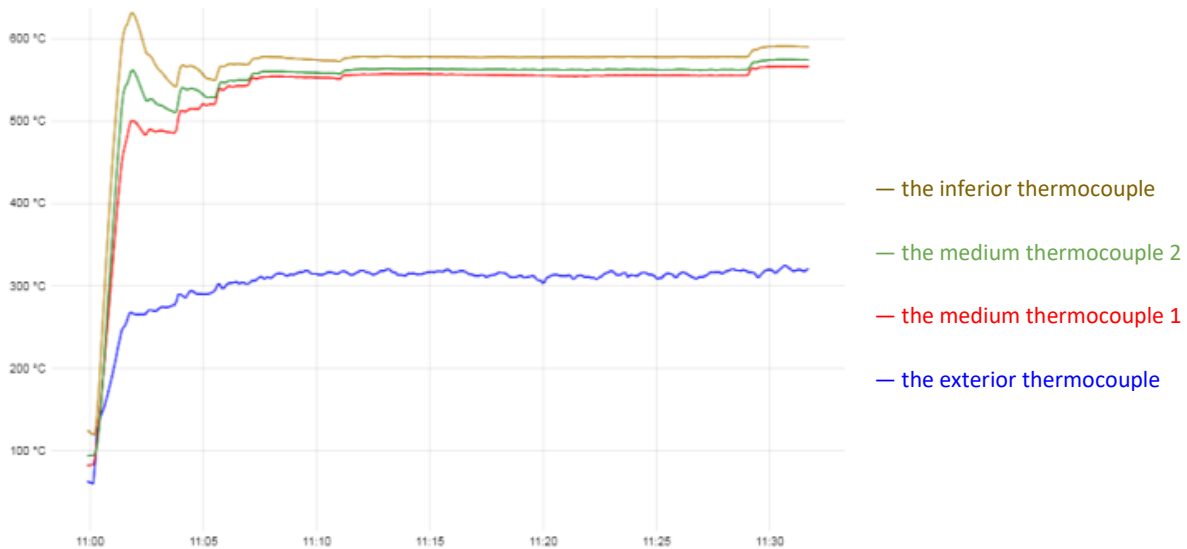


Figure 86: The thermal profile of the first new heat experiment.

The thermal gradient between the two furthest measuring points of this experiment is about only 45 degrees, compared to 60 previously. This could be explained by the use of the thermal insulation wool which has prevented a significant part of the negative effect of air convection on the internal thermal gradient. It can therefore be deduced that the use of insulation between the nozzle and the body of the printer will be very beneficial to limit the large thermal losses related to conduction and convection.

To verify the results obtained, the upper inner thermocouple was exchanged with the outer thermocouple, so the imposed temperature is 315 degrees. The temperature profile for the 4 points of the inner wall is shown in the Figure 87 below:



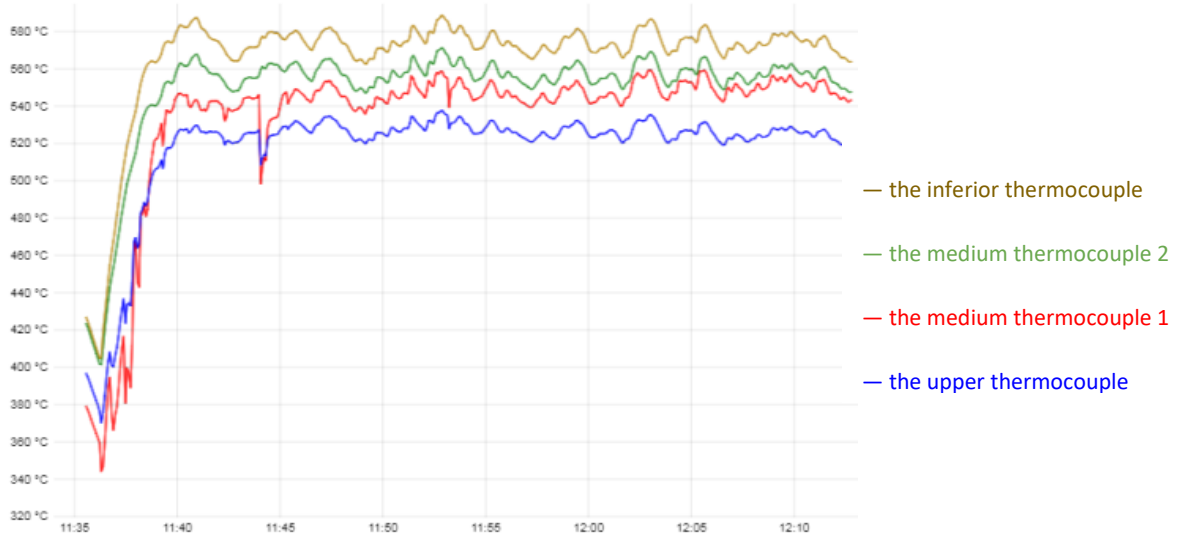


Figure 87: The thermal profile of the second new heat experiment.

Due to the lack of time, unfortunately the insulating layer between the nozzle and the rest of the machine could not be created and an attempt to extrude with the new two-spiral coil without thermal insulation was made but with no positive result. Indeed, as in the case of the second extrusion attempt, it was impossible to control the temperature inside as the convection had affected the thermal profile inside and the material melted again (Figure 88).

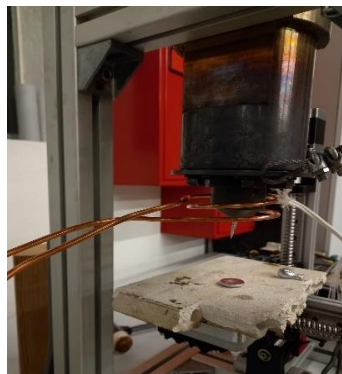


Figure 88: The result of the last extrusion experiment.

## Conclusion

The technology studied in this project, which aims to extrude metallic alloys in the semisolid state using a special 3D printer machine, promises many advantages for the future of Metal AM, including the reduction of production prices and energy saving. However, the different tasks performed throughout this work showed the complexity of successfully controlling the thermal profile in the printer during the alloy extrusion experiments. This difference was demonstrated during the extrusion experiments carried out where, in the various cases treated, the microstructural characterization with OM and SEM showed that the extruded material contains dendrites which confirms that the maintenance of a semi-solid state inside the nozzle (580 degrees) was not possible. The three major reasons that caused these differences between the thermal profiles of the nozzle without and being mounted in the 3D printer are: the complexity of the thermal profile associated to the coil design and nozzle geometry, the convection and the conduction. The next steps to reach the objective of printing the Al 357.0-F in its semisolid state is to create thermal insulation between the nozzle and the rest of the printing system, to minimise the effect of conduction (energy dissipation through the extruder body) and isolation to avoid air convection and its effect on the temperature variation of the nozzle. Additionally, the design of the extruder will be improved in such a way as to be able to better homogenise the thermal profile and stabilise it at temperature values close to 580 degrees.

## References

- [1] AFNOR. – NF E67-001 : Fabrication additive – vocabulaire. Éd, p. 4 (2011).
- [2] Floriane Laverne, Frédéric Segonds, Patrice Dubois, *Fabrication additive - Principes généraux*, (Techniques de l'ingénieur, 2016, ref : BM7017 V2).  
Online: <https://www-techniques-ingenieur-fr.bases-doc.univ-lorraine.fr/res/pdf/encyclopedia/42128210-bm7017.pdf>
- [3] *3D Printing for Beginners – An Introduction*, (CROFT Additive Manufacturing).  
Online: <https://www.croftam.co.uk/3d-printing-for-beginners-an-introduction/>
- [4] Ian Gibson, David Rosen, Brent Stucker, *Additive Manufacturing Technologies - 3D Printing, Rapid Prototyping, and Direct Digital Manufacturing*, (Springer).  
Online: <https://mizaradditive.com/fr/fabrication-additive-etape-etape/>
- [5] Gorka Fernández, *La fabrication additive étape par étape*, (Mizar Additive, 2021).  
Online: <https://mizaradditive.com/fr/fabrication-additive-etape-etape/>
- [6] Gianmaria Cusimano, *Sample car rim*, (GRABCAD Community, 2013).  
Online: <https://grabcad.com/library/sample-car-rim>
- [7] *Qu'est-ce qu'un fichier STL ?*, (3D Systems).  
Online: <https://fr.3dsystems.com/quickparts/learning-center/what-is-stl-file>
- [8] Tatum Anderson, *The application of 3D printing for healthcare*, (ITIJ, 2017).  
Online: <https://www.itij.com/latest/long-read/application-3d-printing-healthcare>
- [9] Mattis Muller, *Design of an induction system for a 3D metallic printer*, (Universitat Politècnica de Catalunya - UPC, 2021).
- [10] Giorgio Magistrelli, *L'outillage et les avantages de la fabrication additive*, (A3DM Magazine, 2017).  
Online: <https://www.a3dm-magazine.fr/magazine/toutes-industries/loutillage-avantages-de-fabrication-additive>
- [11] S. Merkt, C. Hinke, H. Schleifenbaum, H. Voswinckel, *Geometric complexity analysis in an integrative technology evaluation model (ITEM) for selective laser melting (SLM)*, (ResearchGate, 2012). Online:  
[https://www.researchgate.net/publication/262783464\\_Geometric\\_complexity\\_analysis\\_in\\_an\\_integrative\\_technology\\_evaluation\\_model\\_ITEM\\_for\\_selective\\_laser\\_melting\\_SLM](https://www.researchgate.net/publication/262783464_Geometric_complexity_analysis_in_an_integrative_technology_evaluation_model_ITEM_for_selective_laser_melting_SLM)
- [12] Abdellatif Bouzid, Maurice Duval, *Fabrication additive*, (Aluquébec, 2017).  
Online: <https://aluquebec.com/media/1741/ceial-fabrication-additive.pdf>
- [13] AFNOR. – NF ISO 17296-2 : Fabrication additive – Principes généraux – Partie 2 : vue d'ensemble des catégories de procédés et des matières de base. p. 16, 13 juin 2015.
- [14] *About Additive Manufacturing - Directed Energy Deposition*, (Loughborough University).  
Online:  
<https://www.lboro.ac.uk/research/amrg/about/the7categoriesofadditivemanufacturing/directedenergydeposition/>



- [15] Ludvine Cherdo, *Metal 3D printers in 2022: a comprehensive guide*, (Aniwa, 2022).  
Online: <https://www.aniwaa.com/buyers-guide/3d-printers/best-metal-3d-printer/>
- [16] Alexandre Moussion, *Le marché mondial de l'impression 3D atteint les 9,3 milliards de dollars en 2018*, (Primante 3D, 2018).  
Online: <https://www.primante3d.com/chiffres-fabrication-additive-14122018/>
- [17] Michel Suery, *Mise en forme à l'état semi-solide - Rhéoformage et thixoformage*, (Techniques de l'ingénieur, 2010, réf : M3050 V1).  
Online: <https://www-techniques-ingenieur-fr.bases-doc.univ-lorraine.fr/base-documentaire/42476210-mise-en-forme-des-metaux-aspects-rheologiques-et-metallurgiques/download/m3050/mise-en-forme-a-l-etat-semi-solide.html>
- [18] F. Edler, Y G Kim, Graham Machin, Jonathan Pearce, David Rodney White, *Guide on secondary thermometry: specialised fixed points above 0°C*, (ResearchGate, 2017).  
Online: [https://www.researchgate.net/figure/Binary-phase-diagram-for-a-eutectic\\_fig1\\_321885305](https://www.researchgate.net/figure/Binary-phase-diagram-for-a-eutectic_fig1_321885305)
- [19] Shahrooz Nafisi, Reza Ghomashchi, *Semi-Solid Processing of Aluminum Alloys*, (Springer).
- [20] J.-M. Haudin, *Chapitre X : Solidification, Généralités*, (mms2.ensmp, Mines ParisTech - Université PSL).  
Online: [http://mms2.ensmp.fr/mat\\_paris/elaboration/polycop/Ch\\_10\\_Solidif\\_Generalites.pdf](http://mms2.ensmp.fr/mat_paris/elaboration/polycop/Ch_10_Solidif_Generalites.pdf)
- [21] I. Steinbach, C. Beckermann, B. Kauerauf, Q. Li, Jianzheng Guo, *Three-dimensional modeling of equiaxed dendritic growth on a mesoscopic scale*, (ResearchGate, 1999).  
Online: [https://www.researchgate.net/publication/222500871\\_Three-dimensional\\_modeling\\_of\\_equiaxed\\_dendritic\\_growth\\_on\\_a\\_mesoscopic\\_scale](https://www.researchgate.net/publication/222500871_Three-dimensional_modeling_of_equiaxed_dendritic_growth_on_a_mesoscopic_scale)
- [22] Luis Carlos Arias Garcia, *Diseño de un Sistema para evaluar la reología de metal en estado tixotrópico para aplicación en impresión 3D*, (Universitat Politècnica de Catalunya - UPC, 2019).
- [23] David Horwat, *Cours de transformation de phase-Partie II*, (Université de Lorraine).
- [24] Gérard Develey, *Chauffage par induction électromagnétique: principes*, (Techniques de l'ingénieur, 2000, ref : D5935 V1).  
Online: <https://www-techniques-ingenieur-fr.bases-doc.univ-lorraine.fr/base-documentaire/42270210-electrothermie-industrielle/download/d5935/chauffage-par-induction-electromagnetique-principes.html>
- [25] Jean Callebaut, *Chauffage par induction*, (Leonardo energy, 2007).  
Online: [https://www.econologie.com/file/technologie\\_energie/Chauffage\\_par\\_induction.pdf](https://www.econologie.com/file/technologie_energie/Chauffage_par_induction.pdf)
- [26] *Le chauffage par induction électromagnétique*, (Institut National de Recherche et de Sécurité - INRS, 2021).  
Online: <https://www.inrs.fr/media.html?refINRS=ED%204211>
- [27] *Induction Heating*, (Duolin). Online: [https://www.duolin.com/induction\\_heating/](https://www.duolin.com/induction_heating/)
- [28] Casimir Casas, *Extrusor F.CIM Operation Manual*, (PROCOMAME - CMEM, 2021).
- [29] *SR80 Bench Model Welder*, (Peak Sensors).  
Online: <https://peaksensors.co.uk/component-store/production-equipment/sr80-bench-model-welder/>

## Annex A

### Aluminum 357.0-F Casting Alloy

**Categories:** [Metal](#); [Nonferrous Metal](#); [Aluminum Alloy](#); [Aluminum Casting Alloy](#)


**Material Notes:** Data points with the AA note have been provided by the Aluminum Association, Inc. and are NOT FOR DESIGN.

**Composition Notes:**

**Key Words:** Composition information provided by the Aluminum Association and is not for design. Aluminium

357.0-F; UNS A03570; AA357.0-F; Al357.0-F

**Vendors:**

Physical Properties	Metric	English	Comments
Density	2.67 g/cc	0.0965 lb/in <sup>3</sup>	AA; Typical
<b>Mechanical Properties</b>			
Tensile Modulus	72.4 GPa	10500 ksi	(A357.0)
Poissons Ratio	0.33	0.33	Calculated Value (A357.0)
Machinability	50 %	50 %	0-100 Scale (100=best)
Shear Modulus	26.8 GPa	3890 ksi	(A357.0)
<b>Electrical Properties</b>			
Electrical Resistivity	0.00000440 ohm-cm	0.00000440 ohm-cm	AA; Typical 39% IACS Conductivity
<b>Thermal Properties</b>			
Heat of Fusion	389 J/g	167 BTU/lb	Typical for cast aluminum
CTE, linear 	21.4 µm/m-°C @Temperature 20.0 - 100 °C	11.9 µin/in-°F @Temperature 68.0 - 212 °F	AA; Typical
	23.2 µm/m-°C @Temperature 20.0 - 300 °C	12.9 µin/in-°F @Temperature 68.0 - 572 °F	AA; Typical; average over range
Specific Heat Capacity	0.963 J/g-°C	0.230 BTU/lb-°F	
Thermal Conductivity	151 W/m-K	1040 BTU-in/hr-ft <sup>2</sup> -°F	AA; Typical at 25°C
Melting Point	557.2 - 612.8 °C	1035 - 1135 °F	AA; Typical
Solidus	557.2 °C	1035 °F	AA; Typical
Liquidus	612.8 °C	1135 °F	AA; Typical
<b>Processing Properties</b>			
Solution Temperature	540.6 °C	1005 °F	hold at temperature for 8 hr; hot water quench
<b>Component Elements Properties</b>			
Aluminum, Al	91.2 - 93.1 %	91.2 - 93.1 %	As remainder
Copper, Cu	<= 0.05 %	<= 0.05 %	
Iron, Fe	<= 0.15 %	<= 0.15 %	
Magnesium, Mg	0.45 - 0.60 %	0.45 - 0.60 %	
Manganese, Mn	<= 0.03 %	<= 0.03 %	
Other, each	<= 0.05 %	<= 0.05 %	
Other, total	<= 0.15 %	<= 0.15 %	
Silicon, Si	6.5 - 7.5 %	6.5 - 7.5 %	
Titanium, Ti	<= 0.20 %	<= 0.20 %	
Zinc, Zn		<= 0.05 %	<= 0.05 %

[References](#) for this datasheet.

Some of the values displayed above may have been converted from their original units and/or rounded in order to display the information in a consistent format. Users requiring more precise data for scientific or engineering calculations can click on the property value to see the original value as well as raw conversions to equivalent units. We advise that you only use the original value or one of its raw conversions in your calculations to minimize rounding error. We also ask that you refer to MatWeb's [terms of use](#) regarding this information. [Click here](#) to view all the property values for this datasheet as they were originally entered into MatWeb.

# Annex B

